

Heavy quark scattering and quenching in a QCD medium at finite temperature and chemical potential

H. Berrehrah,^{1,*} E. Bratkovskaya,^{1,†} W. Cassing,^{2,‡} P. B. Gossiaux,^{3,§} and J. Aichelin^{3,||}

¹*Frankfurt Institute for Advanced Studies and Institute for Theoretical Physics, Johann Wolfgang Goethe Universität, Ruth-Moufang-Strasse 1, D-60438 Frankfurt am Main, Germany*

²*Institut für Theoretische Physik, Universität Giessen, D-35392 Giessen, Germany*

³*Subatech, UMR 6457, IN2P3/CNRS, Université de Nantes, École des Mines de Nantes, 4 Rue Alfred Kastler, F-44307 Nantes Cedex 3, France*

(Received 6 February 2015; revised manuscript received 30 March 2015; published 7 May 2015)

The heavy quark collisional scattering on partons of the quark gluon plasma (QGP) is studied in a quantum chromodynamics medium at finite temperature and chemical potential. We evaluate the effects of finite parton masses and widths, finite temperature T , and quark chemical potential μ_q on the different elastic cross sections for dynamical quasiparticles (on- and off-shell particles in the QGP medium as described by the dynamical quasiparticle model “DQPM”) using the leading order Born diagrams. Our results show clearly the decrease of the qQ and gQ total elastic cross sections when the temperature and the quark chemical potential increase. These effects are amplified for finite μ_q at temperatures lower than the corresponding critical temperature $T_c(\mu_q)$. Using these cross sections we, furthermore, estimate the energy loss and longitudinal and transverse momentum transfers of a heavy quark propagating in a finite temperature and chemical potential medium. Accordingly, we have shown that the transport properties of heavy quarks are sensitive to the temperature and chemical potential variations. Our results provide some basic ingredients for the study of charm physics in heavy-ion collisions at Beam Energy Scan at RHIC and CBM experiment at FAIR.

DOI: [10.1103/PhysRevC.91.054902](https://doi.org/10.1103/PhysRevC.91.054902)

PACS number(s): 24.10.Jv, 02.70.Ns, 12.38.Mh, 24.85.+p

I. INTRODUCTION

The exploration of the phase diagram of strongly interacting matter is a major field of modern high-energy physics. The transition from hadronic to partonic degrees of freedom at high temperatures or high baryon densities is one of the most interesting challenges of relativistic heavy-ion physics. The discovery of this phase transition is expected to elucidate some of the fundamental aspects of quantum chromodynamics (QCD), i.e., confinement and chiral symmetry breaking. Moreover, the different phases of the QCD phase diagram play an important role in the evolution of the early universe and the structure of the core of neutron stars [1].

The transition from a hadronic to a partonic medium at small net-baryon densities is known to be a crossover. On the other hand, at high baryon densities one expects new phases of strongly interacting matter [2]. In particular, a first-order deconfinement phase transition with a critical endpoint or a chiral symmetry restoration without deconfinement—leading to a quarkyonic phase—may occur at larger baryon densities. Recent results from a statistical analysis of particle ratios measured in Pb+Pb and Au+Au collisions at SchwerIonen-Synchrotron (SIS), Alternating Gradient Synchrotron (AGS), Super Proton Synchrotron (SPS), and Relativistic Heavy-Ion Collider (RHIC) energies point in this direction [3–7]. The phase boundary between quark-gluon and hadronic matter and

the location of the (possible) critical endpoint is suggested by lattice QCD calculations [8,9] to occur for values of μ_B larger than about 400 MeV; for $\mu_B \approx 3\mu_q$ smaller than 400 MeV one expects a smooth crossover from the hadronic to the partonic phase. In addition to this hypothetical first-order transition a rich phase structure might occur at high baryon chemical potential μ_B or quark chemical potential μ_q .

Previous studies have shown that the high-density regime of QCD is accessible with heavy-ion collisions at moderate collision energies [10]. This is supported by the study of the freeze-out points from hadron-gas models as a function of the temperature and chemical potential [11] or hadronic transport models like the hadron-string-dynamics (HSD) approach from [12,13], where the highest baryon densities are predicted for moderate collision energies.

Recent progress in the exciting field of QCD at high baryon densities is driven by new experimental data from the Beam Energy Scan (BES) program at RHIC ($\sqrt{s_{NN}} = 7\text{--}200$ GeV) and NA61 at the SPS ($\sqrt{s_{NN}} = 6.4\text{--}17.4$ GeV). In future experiments of the Compressed Baryonic Matter (CBM) collaboration at FAIR ($\sqrt{s_{NN}} = 2.7\text{--}8.3$ GeV) and the Multi-Purpose Detector (MPD) at NICA ($\sqrt{s_{NN}} = 4\text{--}11$ GeV) will provide additional information. The aim of all these experiments is to explore the QCD phase diagram at high net-baryon densities and moderate temperatures in nucleus-nucleus collisions. This approach is complementary to the studies of matter at high temperatures and low net-baryon densities performed at RHIC and the Large Hadron Collider (LHC) which are designed to study the properties of the deconfined medium at the highest available energy densities (and temperatures). Because lattice QCD (lQCD) does not provide robust results in this regime one has to rely on effective QCD models that match lQCD for $\mu_q = 0$. Furthermore, one

*berrehrah@fias.uni-frankfurt.de

†brat@th.physik.uni-frankfurt.de

‡wolfgang.cassing@theo.physik.uni-giessen.de

§gossiaux@subatech.in2p3.fr

||aichelin@subatech.in2p3.fr

has to look at the characteristics of the medium systematically in terms of collision energy and system size, by studying the strangeness, charm, collective flow, and fluctuations possibly on an event-by-event basis.

Charm physics is one of the promising signals that can be studied at upper FAIR energies. Indeed, both hidden and open charm are expected to contribute to the total charm production also in this energy range. The total charm cross section experimentally is not well known close to threshold and the predictions for A+A rely on parametrizations of experimental data and imply large uncertainties towards threshold. Note that also perturbative QCD (pQCD) calculations show large uncertainties [14]. Therefore, close to the kinematic production thresholds, an unknown territory has to be systematically explored [15,16]. Furthermore, experimental data close to threshold for the elementary charm cross sections have to be taken before more robust conclusions can be expected for p+A and A+A collisions at FAIR/NICA energies. Note that there are presently no p+N data below 20 GeV and no A+A data below top SPS energies for charmonia.

The anomalous suppression of charmonium from screening effects in the quark-gluon plasma (QGP) was predicted to be an experimental signal of the QGP formation by Matsui and Satz [17] because particles containing heavy quarks like charm are produced predominantly in the early stage of the collision due to high kinematical thresholds. Heavy-flavor physics at FAIR thus aims to explore how charm is produced at beam energies close to the kinematical thresholds and how charm propagates in hot and cold nuclear matter as well as in the partonic phase. In addition, the production mechanisms of D and J/ψ mesons will be sensitive to the conditions inside the early fireball.

The scenarios for charm production in A+A collisions based on either hadronic [13,18] or partonic [statistical hadronization model (SHM)] [19] models have given different predictions. Especially the ratio of hidden to open charm ($J/\psi/D$) from the hadronic HSD model [15,16] differs substantially from the one in the partonic SHM model [19] since the $J/\psi/D$ ratio depends on the energy in the c.m.s. (\sqrt{s}) in the first model and is \sqrt{s} independent in the second one. In addition, the $J/\psi/D$ ratio is about one order of magnitude higher in the hadronic than in partonic production scenarios which is due to the much lower threshold for J/ψ production in N+N collisions than for $D + \bar{D}$ pairs. Therefore, the charm production is sensitive to the phases of matter and the ratio of hidden to open charm appears as a very promising probe for the production of charm and its propagation in the medium. In addition the collective flow of charm is expected to provide valuable information on the interaction strength of charm with its medium being of hadronic or partonic nature. Furthermore, it is generally questioned that charm degrees of freedom might achieve a chemical equilibrium in the fireball such that microscopic transport approaches are mandatory to shed some light on the nonlinear charm dynamics.

With the future aim to implement the charm dynamics nonperturbatively into the Parton-Hadron-String Dynamics (PHSD) approach we have to specify the interaction cross sections of the charm degrees of freedom (Q) with the light partonic degrees of freedom incorporated in PHSD, i.e.,

dressed quarks, antiquarks (q, \bar{q}), and gluons (g). Accordingly, in this study we will compute the off-shell cross sections for the reactions $qQ \rightarrow qQ$ and $gQ \rightarrow gQ$ taking into account the quasiparticle nature of the quarks and gluons at finite T and μ_q in PHSD which are adopted from the dynamical quasiparticle model (DQPM) [20–22]. These cross sections are then used to evaluate the energy and momentum losses of a heavy quark as a function of heavy quark momentum, temperature, and quark chemical potential. Our results finally will provide the basic ingredients for the microscopic study of charm physics for the Beam Energy Scan (BES) program at RHIC and the future CBM experiment at FAIR. For a first step in this direction we refer the reader to Ref. [23] where some of the quantities have already been evaluated at $\mu_q = 0$ at finite temperatures relevant at RHIC or LHC energies.

The paper is organized as follows: We first present in Sec. II the basic ingredients needed for the heavy quark scattering in a finite temperature T and quark chemical potential μ_q medium. Therefore, we fix the coupling constant, the parton masses and spectral functions, and the gluon and fermion propagators as given by the DQPM at finite T and μ_q . The analysis of the on- and off-shell kinematics and the calculations of the on- and off-shell elastic cross sections of the scattering of a heavy quark (Q) and light quark (q) and gluon (g) in a partonic medium at finite T and μ_q are specified in Sec. III. In Sec. IV, we calculate the interaction rate of the heavy quark in such a medium. Furthermore, we will perform a quantitative analysis of the heavy quark energy loss (Sec. V) and momentum loss (Sec. VI). Throughout Secs. IV–VI we will point out the effects of finite masses and width, finite temperature, and chemical potential on the heavy quark transport properties. In Sec. VII we summarize the main results and point out their future applications.

II. DYNAMICAL QUASIPARTICLES AT FINITE TEMPERATURE AND CHEMICAL POTENTIAL

The scattering of heavy quarks in vacuum and in a QGP medium in lowest-order QCD perturbation theory (pQCD) was extensively studied in the literature [24,25]. Recent developments reconsidered the concept of perturbatively interacting massless quarks and gluons as constituents of the QGP, which scatter according to the leading (Born) diagrams. The treatment of nonperturbative effects in heavy quark scattering was first carried out by Braaten *et al.* [26–28] in thermal perturbation theory, denoted as the hard thermal loop (HTL) approach and later by Peshier *et al.* [29–31] and Gossiaux *et al.* [32–38]. In Ref. [39] we considered all the effects of the nonperturbative nature of the strongly interacting quark-gluon plasma (sQGP) constituents, i.e., the large coupling, the multiple scattering, etc., where we refrain from a fixed-order thermal loop calculation relying on perturbative self-energies (calculated in the limit of infinite temperature) to fix the in-medium masses of the quarks and gluons and pursue instead a more phenomenological approach. The multiple strong interactions of quarks and gluons in the sQGP are encoded in their effective propagators with broad spectral functions. The effective propagators, which can be interpreted as resummed propagators in a hot and dense QCD

environment, have been extracted from lattice data in the scope of the DQPM [22,40,41].

In this work we extend our study of the scattering processes $qQ \rightarrow qQ$ and $gQ \rightarrow gQ$ in Refs. [23,39] for a partonic medium at finite temperature T and in particular at finite chemical potential μ_q . The gluons (g) and light (q) and heavy (Q) quark masses as well as the fundamental ingredients (infrared regulator “IR” and running coupling “ α_s ”) involved in the scattering amplitudes are determined in the framework of the DQPM. The dependencies of these quantities on T and μ_q will be discussed below.

A. Dynamical quasiparticles at finite temperature and quark chemical potential μ_q

The DQPM describes QCD properties in terms of single-particle Green’s functions [in the sense of a two-particle irreducible (2PI) approach] and leads to the notion of the constituents of the sQGP being strongly interacting massive effective quasiparticles with broad spectral functions (because of the high interaction rates). The strategy for the determination of parton masses and widths within the DQPM approach is to fit the analytical expression of the dynamical quasiparticle entropy density s^{DQP} to the IQCD entropy density “ s^{IQCD} ” which allows one to fix the few parameters present in s^{DQP} by lattice data in equilibrium [20–22,41]. The DQPM describes the general features of QCD at finite temperature (and chemical potential) above $T_c(\mu_q)$. Because it is fitted to IQCD thermodynamics at $\mu_q = 0$, it matches all the QCD symmetries implicitly. Furthermore, it also “roughly” reproduces QCD correlation functions such as transport coefficients (shear and bulk viscosity, electric conductivity, etc.). It is also worth mentioning that no Lagrangian is associated with the DQPM which would allow one to perform calculations for condensates and hadronic amplitudes, etc. Thus, one also should not expect any explicit description of nuclear matter symmetries and properties within the DQPM. Recent NNLO HTL calculations [42] based on the Lagrangian approach can also give a good description of IQCD thermodynamics at finite T and μ assuming the central values of the renormalization scales, with noticeable uncertainties related to the variation of these scales around the central values.

The variation of parton masses as a function of the medium properties is described by the spectral functions which are (except for a factor) identical to the imaginary part of the retarded propagator. These are no longer δ functions in the invariant mass squared (as in the case for bare masses) [40]. For the current analysis, we use the approximation of momentum-independent real and imaginary parts of the retarded self-energy, which are—for a given temperature T —proportional to the parton mass and width, respectively [22]. A partonic propagator Δ is expressed in the Lehmann representation in terms of the spectral function $\Delta(p) = \int \frac{d\omega}{2\pi} \frac{A(\omega, p)}{p_0 - \omega}$. An often used ansatz to model a nonzero width is obtained by replacing the free spectral function $A_0(p) = 2\pi[\delta(\omega - p)^2 - \delta(\omega + p)^2]$ by a Lorentzian form [22,39] which also emerges from Kadanoff-Baym theory in first-order gradient expansion.

The extension of the DQPM to finite quark chemical potential μ_q is more delicate because a guidance by IQCD is

presently very limited. In the simple quasiparticle model one may use the stationarity of the thermodynamic potential with respect to self-energies and (by employing Maxwell relations) derive a partial differential equation for the coupling $g^2(T, \mu_q)$ which may be solved with a suitable boundary condition for $g^2(T, \mu_q = 0)$ [43–46]. Once $g^2(T, \mu_q)$ is known one can evaluate the changes in the quasiparticle masses with respect to T and μ_q , i.e., $\partial M_x^2 / \partial \mu_q$ and $\partial M_x^2 / \partial T$ (for $x = g, q, \bar{q}$) and calculate the change in the “bag pressure” (cf. Refs. [43–47] for details). However, such a strategy cannot be taken over directly in the DQPM because additionally the quasiparticle widths $\gamma_x(T, \mu_q)$ have to be known in the (T, μ_q) plane in this case.

In hard-thermal-loop (HTL) approaches [48,49] the damping of a light quark (or gluon) depends weakly on the quark chemical potential explicitly [50]. This, however, has to be considered with care because HTL approaches primarily address Landau damping and assume small couplings g^2 . Accordingly, these concepts should be applied at sufficiently high temperature, only. Present IQCD calculations suggest that the ratio of pressure to energy density, P/ε , is approximately independent of μ_q as a function of the energy density ε [51]. The functional dependence of the quasiparticle width γ on T and μ_q thus has to be modeled in line with “lattice phenomenology.” We proceed in this paper to some scaling hypothesis to extend the definition of DQPM masses and widths to a finite chemical potential [22]. Assuming three light flavors ($q = u, d, s$) and all chemical potentials to be equal ($\mu_u = \mu_d = \mu_s = \mu_q$) the gluon and light quark masses are taken for T and μ_q as

$$M_g^2(T, \mu_q) = \frac{g^2(T/T_c)}{6} \left(\left(N_c + \frac{1}{2} N_f \right) T^2 + \frac{3}{2} \sum_q \frac{\mu_q^2}{\pi^2} \right),$$

$$M_q^2(T, \mu_q) = \frac{N_c^2 - 1}{8N_c} g^2(T/T_c) \left(T^2 + \frac{\mu_q^2}{\pi^2} \right). \quad (2.1)$$

This functional form is inspired by HTL masses but slightly differs from those to incorporate an explicit scaling with the effective temperature for $N_f = N_c = 3$,

$$T^{*2} = T^2 + \frac{\mu_q^2}{\pi^2}, \quad (2.2)$$

which implies no additional parameter in the DQPM. Thus $M_g^2(T, \mu_q)$ and $M_q^2(T, \mu_q)$ are given by

$$M_g^2(T^*, \mu_q) = \frac{g^2(T^*/T_c(\mu_q))}{6} \left(N_c + \frac{1}{2} N_f \right) T^{*2},$$

$$M_q^2(T^*, \mu_q) = \frac{N_c^2 - 1}{8N_c} g^2(T^*/T_c(\mu_q)) T^{*2}, \quad (2.3)$$

with the coupling constant $g^2(T^*/T_c(\mu_q))$ in (2.3) is considered here as depending on the medium temperature and for

$T^* > T_s$ is given by

$$g^2(T^*, \mu_q) = \frac{48\pi^2}{(11N_c - 2N_f) \ln \left(\lambda^2 \left(\frac{T^*}{T_c(\mu_q)} - \frac{T_s}{T_c(\mu_q)} \right)^2 \right)}. \quad (2.4)$$

The form of the running coupling specified in (2.4) is given for $T > T_c(\mu_q)$. Nevertheless, it seems that this form allows one to describe QCD thermodynamics down to $0.9 T_c(\mu_q)$ as studied in [52]. It is worth mentioning that the scattering and quenching of heavy quarks on light quarks and gluons is carried out in our study only above $T_c(\mu_q)$.

The DQPM masses (2.3) are proportional to $\alpha g(T^*, \mu_q) T^*$ with a certain pre-factor. The coupling $g(T, \mu_q = 0)$ is determined by fitting the DQPM entropy density to the one given by IQCD data and implicitly contains all higher orders in the corresponding HTL masses. This is especially seen in the effective coupling which is strongly enhanced in the infrared. This approach thus does not rely on a perturbative scheme at fixed order but should be interpreted as an approximation to a fully resummed theory (like lattice QCD).

Because the coupling (squared) in the DQPM is a function of T/T_c a straightforward extension of the DQPM to finite μ_q is to consider the coupling as a function of $T^*/T_c(\mu_q)$ with a μ_q -dependent critical temperature,

$$\frac{T_c(\mu_q)}{T_c(\mu_q = 0)} = \sqrt{1 - \alpha \mu_q^2} \approx 1 - \alpha/2 \mu_q^2 + \dots, \quad (2.5)$$

with $\alpha \approx 8.79 \text{ GeV}^{-2}$. The expression of $T_c(\mu_q)$ in (2.5) is obtained by requiring a constant energy density ε for the system at $T = T_c(\mu_q)$ where ε at $T_c(\mu_q = 0) \approx 0.158 \text{ GeV}$ is fixed by lattice QCD calculation at $\mu_q = 0$. The coefficient in front of the μ_q^2 -dependent part at first sight appears arbitrary but can be compared to recent IQCD calculations (for imaginary quark chemical potentials) at finite (but small) μ_B which gives [53]

$$\frac{T_c(\mu_B)}{T_c} = 1 - \kappa \left(\frac{\mu_B}{T_c} \right)^2 + \dots, \quad (2.6)$$

with $\kappa = 0.013(2)$. Rewriting (2.5) in the form (2.6) and using $\mu_B \approx 3\mu_q$ we get $\kappa_{\text{DQPM}} \approx 0.0122$ which compares very well with the IQCD result. Consequently one has to expect an approximate scaling of the DQPM results if the partonic width is assumed to have the form,

$$\begin{aligned} \gamma_g(T, \mu_q) &= \frac{1}{3} N_c \frac{g^2(T^*/T_c(\mu_q))}{8\pi} T \ln \left(\frac{2c}{g^2(T^*/T_c(\mu_q))} + 1 \right), \\ \gamma_q(T, \mu_q) &= \frac{1}{3} \frac{N_c^2 - 1}{2N_c} \frac{g^2(T^*/T_c(\mu_q))}{8\pi} T \\ &\quad \times \ln \left(\frac{2c}{g^2(T^*/T_c(\mu_q))} + 1 \right). \end{aligned} \quad (2.7)$$

This choice leads to an approximate independence of the potential energies per degree of freedom as a function of μ_q . Nevertheless, the conjecture (2.7) should be explicitly controlled by future IQCD studies for $N_f = 3$ at finite quark chemical potential. Unfortunately, this task is presently out of

reach and one has to live with the uncertainty in (2.7) which is assumed in the following investigations.

We recall that within the scaling hypothesis (2.2)–(2.7) the results for the masses and widths at finite T stay about the same as a function of $T^*/T_c(\mu_q)$ when dividing by the temperature T [22].

For a finite quark chemical potential μ_q the energy density ε in the DQPM is seen to scale well with $(T/T_c(\mu_q = 0))^4$ as a function of temperature for $T^*/T_c(\mu_q) > 3$, however, increases slightly with μ_q close to the phase boundary where the scaling is violated on the level of 20%. This violation in the scaling is essentially from an increase of the pressure P [22]. Note that a quark chemical potential of 0.21 GeV corresponds to a baryon chemical potential of $\mu_B \approx 3\mu_q = 0.63 \text{ GeV}$ which is already substantial and the validity of (2.5) becomes questionable. Because the pressure P is obtained from an integration of the entropy density s over temperature T the increase in P with μ_q can directly be traced back to a corresponding increase in entropy density.

Next we discuss the influence of a finite chemical potential μ_q on the running coupling α_s , the DQPM masses, widths, and parton spectral functions. The running coupling $\alpha_s = g^2/(4\pi)$ is presented in Fig. 1(a) as a function of the temperature T for $\mu_q = 0$ and in Fig. 1(b) for finite T and μ_q . One sees that α_s is larger than 1 near $T_c(\mu_q)$ and nonperturbative effects are most pronounced at these temperatures, with $T_c(\mu_q = 0) = 0.158 \text{ GeV}$ and $T_c(\mu_q = 0.2 \text{ GeV}) \approx 0.127 \text{ GeV}$. Note that close to $T_c(\mu_q = 0)$ the full coupling calculated on the lattice increases with decreasing temperature much faster than in the pQCD regime (at high T). A finite μ_q leads to a smaller value of the coupling constant as compared to the $\mu_q = 0$, except close to the corresponding critical temperature $T_c(\mu_q)$. Indeed, the value of $\alpha_s(T_c(\mu_q = 0)) = 2.84$ while $\alpha_s(T_c(\mu_q = 0.2 \text{ GeV})) = 4.7$. For temperatures larger than $T_c(\mu_q = 0)$ one finds systematically $\alpha_s(T, \mu_q = 0) > \alpha_s(T, \mu_q)$, as shown in Fig. 1(b).

The DQPM masses and widths for the gluon (g) and light quarks (q), given by (2.1) and (2.7), are presented in Figs. 2(a) and 2(b), respectively. Because the width is found to be much smaller as the pole mass, the excitations can well be considered as dynamical (off-shell) quasiparticles. For larger T , after a shallow minimum at $T \approx 1.2T_c(\mu_q)$, the width γ increases slowly with T and even for large T is to a good accuracy proportional to the temperature (and also to the mass).

In Figs. 2(a) and 2(b), the masses and widths are plotted as a function of the temperature. It is seen that the gluon and light quark masses and widths decrease at fixed T with increasing quark chemical potential μ_q . The finite μ_q has a larger effect on the masses as compared to the widths. For completeness we note $T_c(\mu_q = 0) = 0.158 \text{ GeV}$, $T_c(\mu_q = 0.2 \text{ GeV}) = 0.127 \text{ GeV}$, and $T_c(\mu_q = 0.3 \text{ GeV}) = 0.072 \text{ GeV}$.

Using the pole masses and widths (2.1) and (2.7) and the DQPM running coupling (cf. Fig. 1), the Breit-Wigner spectral functions for the different QGP species are completely determined, i.e., the imaginary parts of the retarded propagators. Accordingly, also the full retarded propagators for the effective partonic degrees of freedom are known in first-order gradient

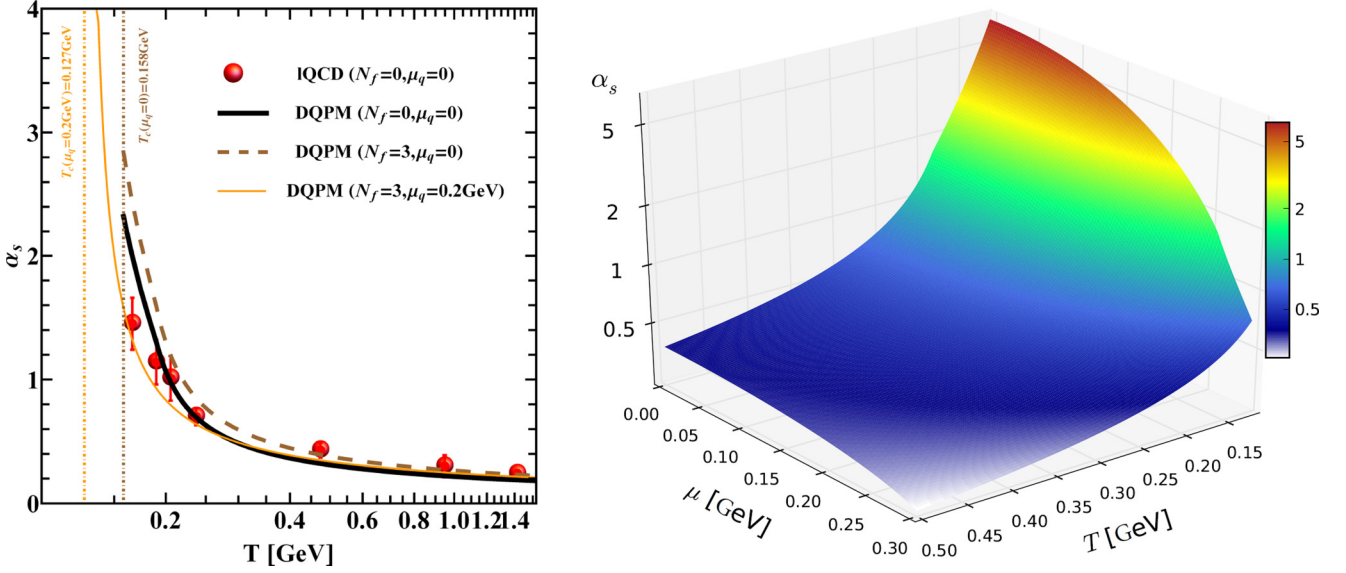


FIG. 1. (Color online) (left) The DQPM running coupling $\alpha_s(T, \mu_q) = g^2(T^*/T_c(\mu_q))/(4\pi)$ as a function of T in the IQCD for $N_f = 0$ (red spheres) [54] and in the DQPM at zero chemical potential for $N_f = 0$ (black line) and $N_f = 3$ (dashed brown line). The result for the DQPM at finite quark chemical potential ($\mu_q = 0.2$ GeV) for $N_f = 3$ is given by the orange thin line, (right) 3D plot of $\alpha_s(T, \mu_q)$.

expansion and we can proceed with the calculation of some amplitudes keeping in mind the uncertainties at high μ_q .

III. qQ AND gQ ELASTIC SCATTERING AT FINITE T AND μ_q

The matrix elements for the $qQ \rightarrow qQ$ and $gQ \rightarrow gQ$ channels have been calculated for the case of massless partons in the vacuum in Refs. [24,25]. In this section we study the qQ and gQ elastic scattering in the QGP medium at finite temperature T and chemical potential μ_q considering the case of on- and off-shell gluons and light and heavy quarks. The partons are dressed by effective masses in the on-shell case

and are dressed by the DQPM spectral functions with a finite width in the off-shell case. We refer to the on-shell study as the DpQCD approach (Dressed pQCD) and to the off-shell case as the IEHTL approach (Infrared Enhanced Hard Thermal Loop). For the DpQCD approach the qQ and gQ elastic cross section at finite T and μ_q is determined by using (i) the running coupling $\alpha_s(T, \mu_q)$ (Fig. 1), and (ii) the DQPM pole masses for the incoming and outgoing quarks and gluons. The DQPM gluon pole mass serves also as an infrared regulator in the gluon propagator.

Considering in- and out- dynamical quasiparticles (DQP), the corresponding quasielastic IEHTL cross section σ^{IEHTL} for the process $(1)^{m(1)} + (2)^{m(2)} \rightarrow (3)^{m(3)} + (4)^{m(4)}$ is deduced by

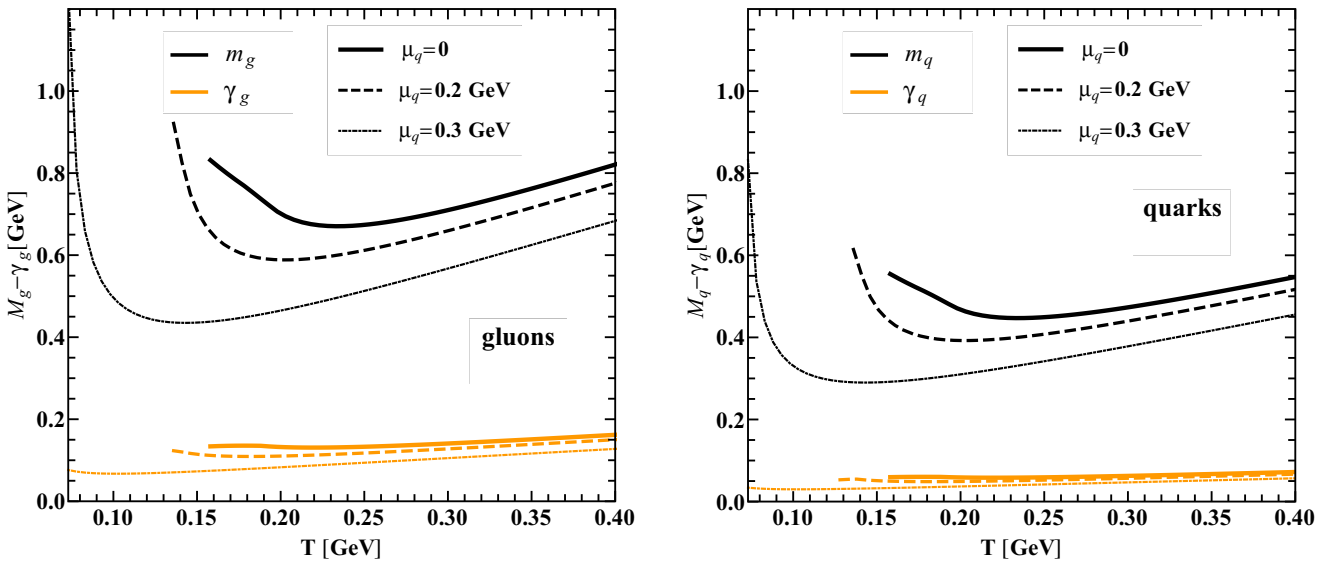


FIG. 2. (Color online) The DQPM pole masses and widths for the gluons (M_g, γ_g) (left) and light quarks (M_q, γ_q) (right) given by (2.1) and (2.7) as a function of temperature for different values of the quark chemical potential μ_q .

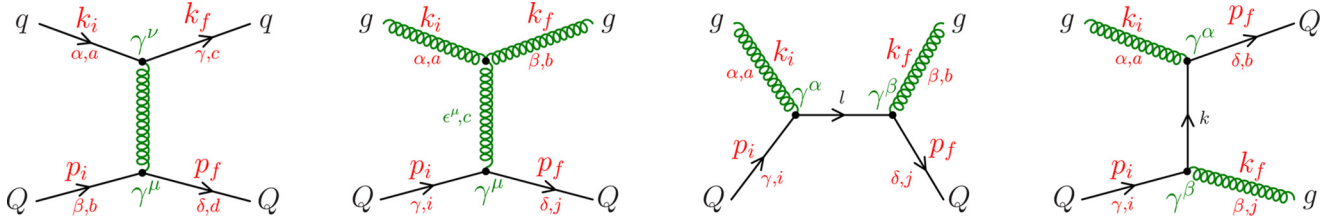


FIG. 3. (Color online) Feynman diagrams for the $qQ \rightarrow qQ$ and $gQ \rightarrow gQ$ scattering process. Latin (Greek) subscripts denote color (spin) indices. k_i , respectively, p_i (k_f , respectively, p_f) denote the initial (final) 4-momentum of the light quark or the gluon, respectively, the heavy quark. The invariant energy squared is given by $s = (p_i + k_i)^2$, $t = (p_i - p_f)^2$, $u = (p_i - k_f)^2$.

the convolution of the modified pQCD cross section σ , where complex propagators are considered in the transition matrix elements, with the spectral functions, i.e.,

$$\begin{aligned} \sigma^{\text{IEHTL}}(s) &= \int dm^{(1)} dm^{(2)} dm^{(3)} dm^{(4)} \\ &\times \sigma(s, m^{(1)}, m^{(2)}, m^{(3)}, m^{(4)}) \rho_{(1)}^{\text{BW}}(m^{(1)}) \rho_{(2)}^{\text{BW}}(m^{(2)}) \\ &\times \rho_{(3)}^{\text{BW}}(m^{(3)}) \rho_{(4)}^{\text{BW}}(m^{(4)}), \end{aligned} \quad (3.1)$$

where $\rho_{(i)}^{\text{BW}}(m^{(i)})$ is the Breit-Wigner spectral function of the particle i , normalized as $\int_0^\infty dm^{(i)} \rho_{(i)}^{\text{BW}}(m^{(i)}) = 1$. The on- and off-shell cross sections for qQ , gQ scattering in the sQGP at finite T and μ_q are obtained using the DQPM parametrizations for the quark (gluon) self-energies, spectral functions, and interaction strength at finite T and μ_q . Here, in principle, a two-particle correlator should appear, but because we work in a 2PI motivated scheme the partons in the sQGP can be characterized by (dressed) single-particle propagators (cf. Ref. [23]).

In the context of the hot and dense QGP, the elementary Feynman diagrams for the qQ and gQ elastic scattering at order $O(\alpha_s)$ are illustrated in Fig. 3.

A. On- and off-shell qQ elastic scattering

The process $qQ \rightarrow qQ$ is calculated here to lowest order in the perturbation expansion using the extended Feynman rules for massless quarks in Politzer's review [55] for the case of finite masses and widths. The color sums are evaluated using the techniques discussed in Ref. [55]; the spin sums will be discussed below. Contrary to the case of massless gluons where the “transverse gauge” is used, the “Lorentz covariance” is used for the case of massive gluons here because a finite mass in the gluon propagator allows one to fix the 0th components of the gluon fields A_a^0 ($a = 1, \dots, 8$) by the spatial degrees of freedom A_a^k ($k = 1, 2, 3$). Furthermore, the divergence encountered in the t channel (Ref. [24,25,56])—when calculating the total cross sections σ^{qQ} and σ^{gQ} —is cured self-consistently in the DpQCD and IEHTL models because the infrared regulator is given by the finite DQPM gluon mass (and width) in the DpQCD (IEHTL) model. For on-shell qQ elastic scattering, the t -channel invariant squared amplitude—averaged over the initial spin and color degrees of freedom and summed over the final state spin and color— \mathcal{M}_t

is given by

$$\begin{aligned} \sum |\mathcal{M}_t|^2 &= \frac{4g^4}{9(t - m_g^2)^2} [(s - M_Q^2 - m_q^2)^2 \\ &+ (u - M_Q^2 - m_q^2)^2 + 2(M_Q^2 + m_q^2)t], \end{aligned} \quad (3.2)$$

where m_q (M_Q) is the light quark (heavy quark) mass and m_g is the DQPM exchanged gluon mass.

In the off-shell picture we take into account not only the finite masses of the partons, but also their spectral functions, i.e., their finite widths. Because the light quark and heavy quark masses change before and after the scattering (“quasielastic” process) we introduce the mass m_q^i for the initial q and m_q^f for the final q , and allow for different masses of the heavy quark, M_Q^i for the initial Q and M_Q^f for the final Q . The squared amplitude—averaged over the initial spin and color degrees of freedom and summed over the final state spin and color—gives

$$\begin{aligned} \sum |\mathcal{M}|^2 &= \frac{2g^4}{9[(t - m_g^2)^2 + 4\gamma_g^2 q_0^2]} \\ &\times \left[4 \left(p_f^\mu p_i^\nu + p_i^\mu p_f^\nu + g^{\mu\nu} \frac{t}{2} \right) \right] \\ &\times \left[4 \left(k_{f,\mu} k_{i,\nu} + k_{i,\mu} k_{f,\nu} + g_{\mu\nu} \frac{t}{2} \right) \right], \end{aligned} \quad (3.3)$$

where we have incorporated the DQPM propagators (i.e., $t_\pm^* = t - m_g^2 \pm 2i\gamma_g q_0$, with m_g , γ_g is, respectively, the effective gluon mass and total width at temperature T and quark chemical potential μ_q and $q^0 = p_f^0 - p_i^0 = k_f^0 - k_i^0$ is the gluon energy in the t channel). Thus the divergence in the gluon propagator in the t channel is regularized.

The relative contribution of the off-shell partons to the pQCD cross section is expected to change because of different kinematical thresholds and to the changes in the matrix element, corresponding to the diagram in Fig. 3. The off-shell kinematical limits for the momentum transfer squared t and the expressions of the Mandelstam variables in the case of off-shell heavy quark scattering are given in Ref. [39].

B. On- and off-shell gQ elastic scattering

The invariant amplitudes for the three graphs (shown in Fig. 3) for the case of massive heavy quarks and massless gluons is given according to Combridge [25] and revisited in [39]. In Ref. [39] we have already studied the scattering of massive on- and off-shell heavy quarks on massive on- and

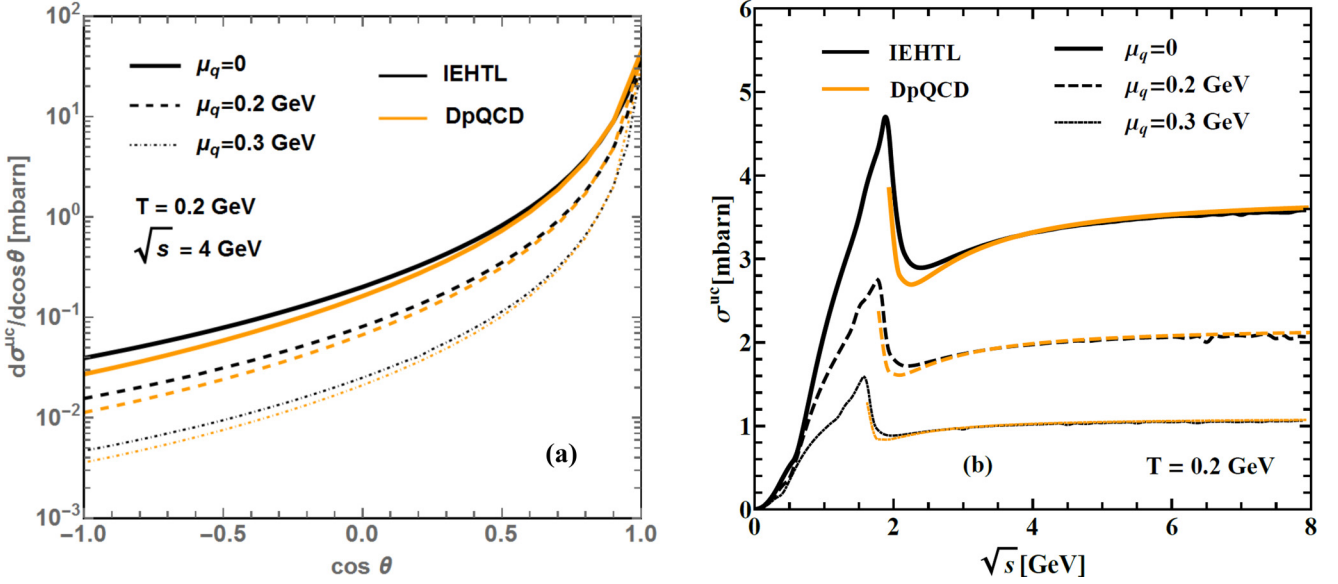


FIG. 4. (Color online) Differential (a) and total (b) elastic cross section for $uc \rightarrow uc$ elastic scattering for off-shell (black lines) and on-shell partons (orange lines) at three different values of the quark chemical potential μ_q (see legend) at $T = 0.2$ GeV. We consider the DQPM pole masses for the on-shell partons and the DQPM spectral functions for the off-shell degrees of freedom.

off-shell gluon in a finite temperature medium at $\mu_q = 0$. In this paper we extend this study to a medium at finite temperature and chemical potential. Therefore, the lowest-order amplitude for the process $gQ \rightarrow gQ$, obtained from the Feynman rules of the gauge theory by the sum of the amplitudes of the three graphs (cf. Appendix A.4 of [39]), where to obtain the correct result for the squared matrix element,

$$\langle |\mathcal{M}|^2 \rangle = \frac{1}{4} \sum_{\text{spins}} T_{\alpha\beta} T_{\alpha'\beta'}^* \varepsilon_i^\alpha \varepsilon_i^{*\alpha'} \varepsilon_f^\beta \varepsilon_f^{*\beta'}, \quad (3.4)$$

we have to use appropriate projection operators for the transverse polarization states,

$$\begin{aligned} \sum_{\text{pol}, i} \varepsilon_{i,\alpha} \varepsilon_{i,\alpha'} &= g_{\alpha\alpha'} - \frac{k_{i,\alpha} k_{i,\alpha'}}{(m_g^i)^2}, \\ \sum_{\text{pol}, f} \varepsilon_{f,\beta} \varepsilon_{f,\beta'} &= g_{\beta\beta'} - \frac{k_{f,\beta} k_{f,\beta'}}{(m_g^f)^2}. \end{aligned} \quad (3.5)$$

We recall that for vector fields with nonzero Lagrangian mass there is no gauge freedom anymore. The massive vector field A_μ only has to fulfill the condition $\partial^\mu A_\mu = 0$. Therefore, the sum over the initial and final gluon polarizations is fixed by the expressions in (3.5).

For the case of finite masses and widths of the scattering quarks and gluons, the gQ elastic scattering amplitude was given in Ref. [39], where we have to take into account the spectral functions for the heavy quark and gluon masses at finite temperature and chemical potential, the coupling (cf. Fig. 1) at finite T and μ_q and the quark and gluon propagators for the case of massive vector gluons with finite lifetime $G_F^{\mu\nu}(q, m_g)$ and for the case of massive fermions with finite

lifetime $S_F(p, m_q)$:

$$\begin{aligned} G_F^{i,\mu\nu}(q) &= -i \frac{g^{\mu\nu} - q^\mu q^\nu / m_g^2}{t - m_g^2 + i2\gamma_g(p_0^i - p_0^f)}, \\ S_F^u(p) &= \frac{\not{p} + M_Q}{u - M_Q^2 + i2\gamma_Q(p_0^i - k_0^f)}, \\ S_F^s(p) &= \frac{\not{p} + M_Q}{s - M_Q^2 + i2\gamma_Q(p_0^i + p_0^f)}, \end{aligned} \quad (3.6)$$

where m_g , γ_g (M_Q , γ_Q) are the mass and width of the gluon or the heavy quark at finite temperature and chemical potential (cf. Sec. II). We note that the heat bath breaks the Lorentz covariance. Accordingly the energies p_0^i and p_0^f denote quantities in the rest frame of the heat bath.

C. Results for elastic scatterings

We consider first the scattering of a (high momentum) heavy quark with a light quark or a gluon in a QGP at temperature $T = 0.2$ GeV with invariant energy $\sqrt{s} = 4$ GeV for different quark chemical potential $\mu_q = 0, 0.2, 0.3$ GeV. Figure 4(a) presents the off-shell differential cross section $d\sigma/d \cos \theta$ (black lines) in comparison to the on-shell cross section (orange lines) of the uc elastic scattering. The importance of finite width corrections in the uc scattering processes is illustrated by comparing the two differential cross sections. For the energy of $\sqrt{s} = 4$ GeV one observes a deviation of the off-shell results compared to the on-shell ones only for large scattering angles. However, according to the small differences between the differential on- and off-shell cross sections one can conclude that the total on-shell cross sections do not change on a relevant scale when introducing off-shell masses. This is particularly important because the width of the heavy quark was taken as an upper limit (cf. Sec. II). Figure 4(a) shows also the influence of a finite

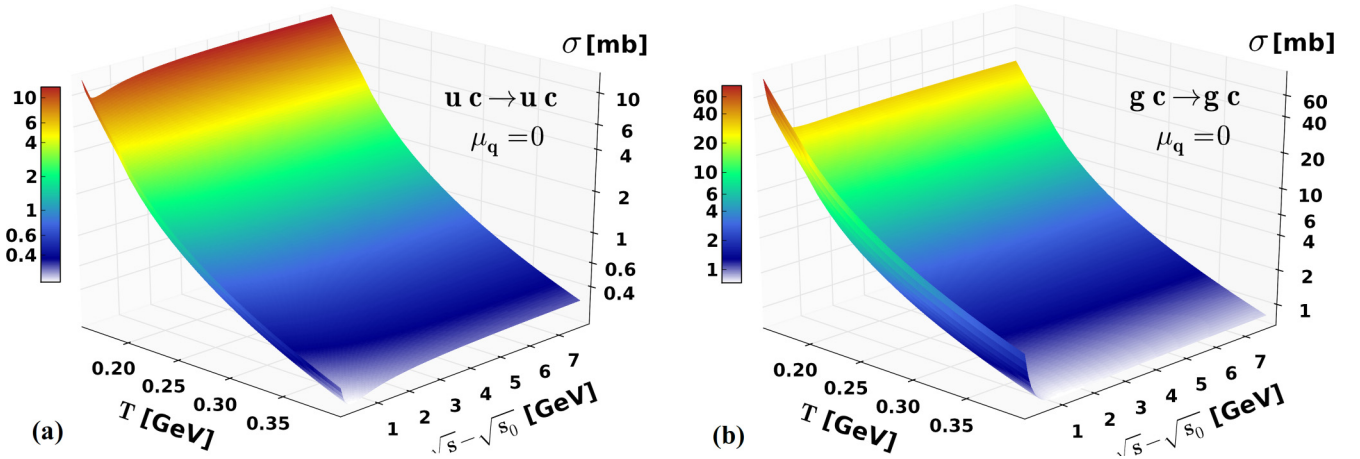


FIG. 5. (Color online) Elastic cross section of $uc \rightarrow uc$ (a) and $gc \rightarrow gc$ (b) scattering as a function of the temperature T and the invariant energy above threshold $\sqrt{s} - \sqrt{s_0}$, where $\sqrt{s_0}$ is the threshold energy, for on-shell partons as described by the DpQCD approach at $\mu_q = 0$.

chemical potential on the heavy quark scattering. The increase of μ_q leads to a decrease of $d\sigma/d\cos\theta$ and consequently to a decrease of the total cross section as illustrated in Fig. 4(b). Despite the lower value of the IR regulator at higher values of μ_q (decrease of the gluon mass at finite μ_q) the smaller values of the running coupling at finite μ_q explain the decrease of $d\sigma/d\cos\theta$ at finite and large values of μ_q .

The total elastic cross section of a c quark, which traverses a plasma at temperatures $T = 0.2$ GeV, as calculated in the DpQCD and IEHTL approaches, is shown in Fig. 4(b) as a function of \sqrt{s} for different values of μ_q . Apart for energies close to the threshold the cross sections show a somewhat smooth dependence on the invariant energy \sqrt{s} , however, differ substantially in magnitude with temperature and chemical potential. Figure 4(b) demonstrates also that, independently on μ_q , the off-shell mass distributions only have a sizable impact at the threshold given by the pole masses for uc scattering. This is because of the moderate parton widths considered in the DQPM model. At energies below the on-shell threshold the off-shell cross section increases with \sqrt{s} because more and more masses can contribute. Whereas the on-shell cross section diverges at the threshold the off-shell cross section shows a maximum at the on-shell threshold and decreases then due to the decrease of the on-shell cross section.

The conclusions drawn before for the study of uc elastic scattering are valid also for gc scattering, however, with cross sections for gQ elastic scattering that are larger than the cross sections for uc scattering by roughly a factor of 9/4 which is a ratio of the different color Casimir operators (squared). This is also related to the fact that the scattering of heavy quarks with gluons proceeds via t , s , and u channels, whereas one has only the t channel for uc elastic scattering.

Figures 5(a) and 5(b) show explicitly the temperature and \sqrt{s} dependencies of the uc and gc elastic cross sections at $\mu_q = 0$, as described in the DpQCD approach. We deduce that an increasing medium temperature T leads to an increase of the thermal gluon mass (infrared regulator) and hence to a decrease of the DpQCD uc and gc elastic cross sections. The effective gluon mass is roughly proportional to T for temperatures above 0.2 GeV. The large enhancement of the total cross section for

temperatures close to $T_c(\mu_q)$ can be traced back to the infrared enhanced coupling in the DpQCD/IEHTL models.

To quantify the effect of a finite μ_q on the heavy quark scattering, we show in Figs. 6(a) and 6(b) the uc and gc thermal transition rate ω [defined by Eq. (3.8) in Ref. [23]] as a function of T and μ_q . We provide the results only for DpQCD because there is just a small difference between the on-shell DpQCD and the off-shell IEHTL approaches (cf. Fig. 4).

There are two different profiles in the (T, μ_q) dependencies of the thermal transition rate ω . For temperatures larger than $T_c(\mu_q = 0) = 0.158$ GeV, a small effect of a finite μ_q , leading to a decrease of ω , is noticed. For temperatures smaller than $T_c(\mu_q = 0)$, an increase of ω appears when μ_q increases. The last effect is due to the increase of the coupling α_s at these temperatures. More precisely, one has $\alpha_s(T < T_c(\mu_q = 0), \mu_q) > \alpha_s(T = T_c(\mu_q = 0), \mu_q)$. In addition to the transition amplitudes, one should also consider the effect of the statistical weights f_{uc}^{FD} (Fermi-Dirac distribution function) at finite (T, μ_q) in the evaluation of ω ; f_{uc}^{FD} increases for large values of μ_q leading to an extra contribution to the increase of the thermal transition rate ω for $T < T_c(\mu_q = 0)$, but is not enough to counterbalance the decrease of the total cross section for $T > T_c(\mu_q = 0)$.

The thermal transition rate can be parametrized by a power law in T for each value of μ_q , i.e., $\sim T^{-\beta}$ for $T > T_c(\mu_q = 0)$. In fact, one can find that $\beta^{T_c(\mu_q=0) < T < 1.2T_c(\mu_q)} \sim 4, \beta^{T > 1.2T_c(\mu_q)} \sim 2$. These different power laws in T will have a sizable effect on the transport coefficients to be evaluated in the following sections. On the other hand, having almost the same power laws at finite μ_q as compared to $\mu_q = 0$ [for temperatures larger than $T_c(\mu_q = 0)$] leads to some scaling effects in the transport coefficients at these temperatures.

Additionally, it is worth evaluating the uc and gc elastic scattering cross section as a function of the energy density ε available in the heavy-ion collisions because out-of-equilibrium a temperature is ill defined while ε can be well calculated in the local rest frame (e.g., in PHSD). Here the energy density ε for a given temperature T and quark chemical potential μ_q is obtained by using the inverted DQPM equation of state which gives the temperature as a function of the energy density ε

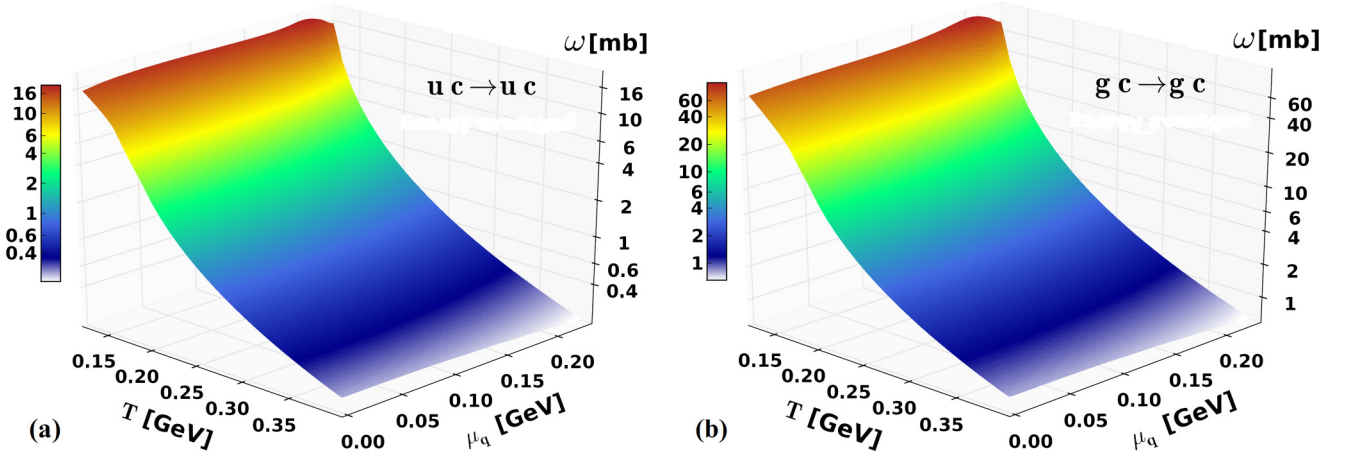


FIG. 6. (Color online) Thermal transition rate ω of $uc \rightarrow uc$ (a) and $gc \rightarrow gc$ (b) as a function of the temperature T and quark chemical potential μ_q for on-shell partons as described by the DpQCD approach.

for a given quark chemical potential. The temperature as a function of ε for $\mu_q = 0, 0.1, 0.2$ GeV is shown in Fig. 7(a). Note that the DQPM model describes the QCD energy density at temperatures even as low as $T \sim T_c(\mu_q)$.

Transport theoretical simulations have shown that the local energy densities achieved in the course of heavy-ion collisions at FAIR energies reach at most 3 GeV fm^{-3} , at SPS and RHIC energies up to 30 GeV fm^{-3} , and up to 300 GeV fm^{-3} at LHC. Therefore one observes that the uc elastic cross section, displayed in Fig. 7(b) at the energy densities of interest is $\in [0.08\text{--}8]$ mb from LHC to FAIR energies, following the DpQCD/IEHTL approaches, with typical values of 5 mb at the phase transition line.

Finally, we note that we did not consider yet the radiative energy loss in our study because we expect that, from the large gluon mass in the DQPM, the radiative processes are subdominant as compared to the collisional ones, especially for low heavy quark momenta (p_T) which can only be generated in heavy-ion collisions at FAIR/NICA energies. We mention that in a more recent transport study—incorporating the cross sections calculated here—by Song *et al.* [57] it was shown that up to transverse momenta of about 6 GeV/c at the top RHIC energy the charm $R_{AA}(p_T)$ is compatible with experimental observation including only the collisional energy loss. Accordingly, the radiative energy loss of charm quarks might be neglected especially at much lower bombarding energies. On the other hand we expect the radiative energy loss to dominate at very high p_T as accessible at the LHC, however, we do not address such systems at $\mu_q = 0$ here.

IV. HEAVY QUARK INTERACTION RATES IN A MEDIUM AT FINITE T AND μ_q

Using the elastic cross section for $q(\bar{q})Q$ and gQ collisions, for on- and off-shell partons—as calculated in Sec. III—we evaluate the interaction rate of a heavy quark with momentum \mathbf{p} and energy E propagating through a QGP in thermal and chemical equilibrium at a given temperature T and quark chemical potential μ_q . The quarks/antiquarks

of the plasma are described by a Fermi-Dirac distribution $f_{q,\bar{q}}(\mathbf{q}) = \frac{1}{e^{(E_q \mp \mu_q)/T} + 1}$ whereas the gluons follow a Bose-Einstein distribution $f_g(\mathbf{q}) = \frac{1}{e^{E_g/T} - 1}$.

For on-shell particles (DpQCD model) and in the reference system in which the heavy quark has the velocity $\boldsymbol{\beta} = \mathbf{p}/E$ the (on-shell) interaction rate $R^{\text{on}}(\mathbf{p}) = \frac{dN_{\text{coll}}^{2 \rightarrow 2}}{dt}$ for $2 \rightarrow 2$ collisions is given by [23]

$$R^{\text{on}}(\mathbf{p}, T, \mu_q) = \sum_{q,\bar{q},g} \frac{M_Q}{16(2\pi)^4 E} \int \frac{q^3 m_0^{\text{on}}(s) f_r(\mathbf{q})}{s E_q} dq, \quad (4.1)$$

where $\sum_{q,\bar{q},g}$ denotes the sum over the light quarks or antiquarks and gluons of the medium. In Eq. (4.1) $f_r(\mathbf{q})$ is the invariant distribution of the plasma constituents in the rest frame of the heavy quark, given for the quark/antiquark by

$$\int d\Omega f_r(\mathbf{q}) = 2\pi \int d\cos\theta_r \frac{1}{e^{(u^0 E_q - u \cdot \mathbf{q} \cos\theta_r \mp \mu_q)/T} + 1}, \quad (4.2)$$

with $u \equiv (u^0, \mathbf{u}) = \frac{1}{M_Q}(E, -\mathbf{p})$ being the fluid 4-velocity measured in the heavy quark rest frame, while θ_r is the angle between \mathbf{q} and \mathbf{u} . $m_0^{\text{on}}(s)$ in (4.1) is related to the transition amplitude $|\mathcal{M}_{2,2}|^2$ of the collision $q(\bar{q}, g)Q \rightarrow q(\bar{q}, g)Q$ by

$$m_0^{\text{on}}(s) = \frac{1}{2p_{cm}^2(s)} \int_{-4p_{cm}^2}^0 \frac{1}{g_Q g_p} \times \sum_{i,j} \sum_{k,l} |\mathcal{M}_{2,2}(s, t; i, j | k, l)|^2 dt, \quad (4.3)$$

with $p_{cm} = (q M_Q)/\sqrt{s}$ denoting the momentum of the scattering partners in the c.m. frame and g_Q (g_p) the degeneracy factor of the heavy quark (parton).

For off-shell partons (IEHTL model) the elastic interaction rate is obtained by replacing

$$\int \frac{d^3 p}{(2\pi)^3} \frac{1}{2E} \rightarrow \int \frac{d^4 p}{(2\pi)^4} \rho(p) \Theta(p_0), \quad (4.4)$$

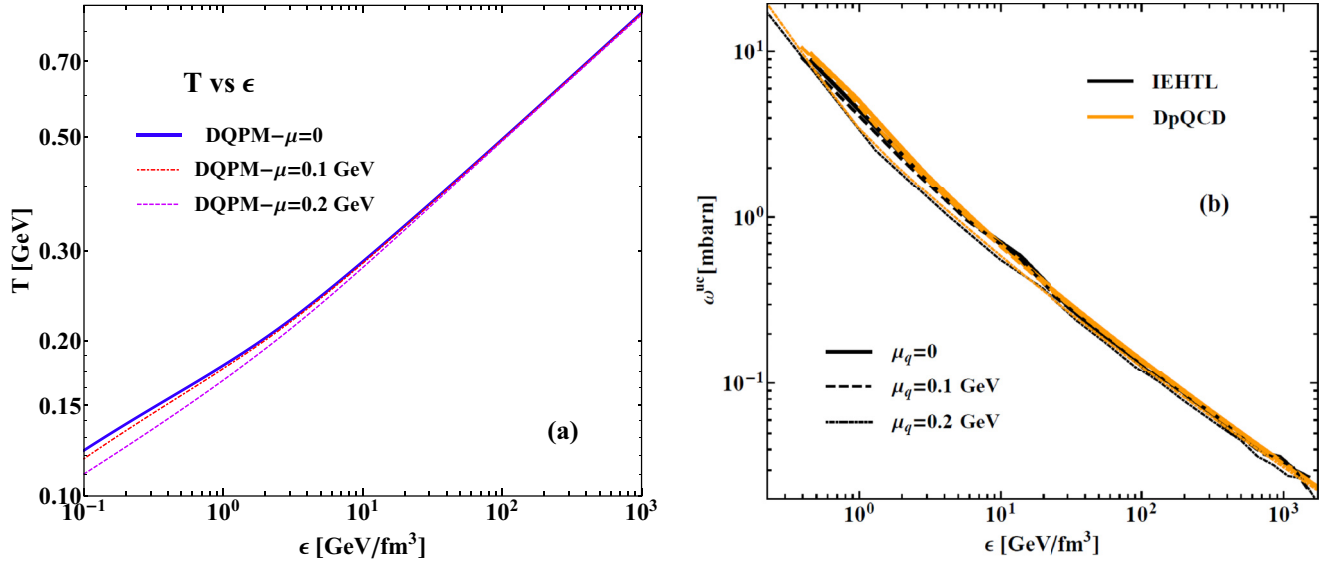


FIG. 7. (Color online) (a) Temperature T as a function of the energy density ϵ from the DQPM for different values of the quark chemical potential μ_q . (b) Thermal transition rate for $uc \rightarrow uc$ scattering for off-shell (IEHTL) and on-shell (DpQCD) partons as a function of the energy density ϵ .

with $\rho(p)$ denoting the spectral function which can be specific for each particle species. For the Breit-Wigner- m form of the spectral function, the explicit extension of Eq. (4.1) for the off-shell case is given by

$$R^{\text{off}}(\mathbf{p}, T, \mu_q) = \sum_{q, \bar{q}, g} \Pi_{i \in p, q, p', q'} \int m_i dm_i \rho_i^{\text{BW}}(m_i) \frac{m_p}{16(2\pi)^4 E} \times \int \frac{q^3 m_0^{\text{off}}(s) f_r(q)}{s E_q} dq, \quad (4.5)$$

where

$$m_0^{\text{off}}(s) = \frac{1}{2p^i p^f} \int_{t_{\min}}^{t_{\max}} \frac{1}{g_p g_Q} \sum_{i, j} \sum_{k, l} |\mathcal{M}_{2,2}^{\text{off}}(s, t; i, j | k, l)|^2 dt, \quad (4.6)$$

with $\sum |\mathcal{M}_{2,2}^{\text{off}}(p, q; i, j | p', q'; k, l)|^2(s, t)$ being the off-shell transition amplitude defined in the IEHTL approach (cf. Ref. [39]); p^i (p^f) is the initial (final) heavy quark momentum and the integration boundaries t_{\min} and t_{\max} are given by

$$t_{\min}^{\max} = -\frac{s}{2}(1 - (\beta_1 + \beta_2 + \beta_3 + \beta_4) + (\beta_1 - \beta_2)(\beta_3 - \beta_4) \pm \sqrt{(1 - \beta_1 - \beta_2)^2 - 4\beta_1\beta_2} \sqrt{(1 - \beta_3 - \beta_4)^2 - 4\beta_3\beta_4}),$$

$$\text{with: } \beta_1 = (m_q^i)^2/s, \quad \beta_2 = (M_Q^i)^2/s, \quad \beta_3 = (m_q^f)^2/s, \quad \beta_4 = (M_Q^f)^2/s. \quad (4.7)$$

The total interaction rate (4.5) of the off-shell approach (IEHTL) in the plasma rest system is compared to that of the on-shell calculations (DpQCD) (4.1) in Fig. 8(a) as a function of the momentum of the heavy quark p for different values of the quark chemical potential μ_q at $T = 0.2$ GeV. We assume here a Breit-Wigner spectral function and a Boltzmann-Jüttner distribution for both the light quarks/antiquarks and the gluons. Our results are somewhat independent of the choice of the spectral function or by replacing the Boltzmann-Jüttner distribution by a Fermi/Bose distribution. In Fig. 8(a) the black lines refer to IEHTL results and the orange lines to DpQCD results. We see from Fig. 8(a) that the finite width of the spectral function (with the DQPM width) decreases the interaction rate of heavy quarks with the medium on the order of 20%. This modification is somewhat independent of the heavy quark momentum, temperature, and quark chemical potential of the plasma. The difference between the DpQCD and IEHTL rates is related on one side to the propagator, which

contains an additional imaginary part proportional to the gluon width in the IEHTL model, and on the other side to the energy asymmetric contribution of the Breit-Wigner spectral function in IEHTL.

For fixed temperature $T = 0.3$ GeV the variation of the quark chemical potential μ_q from $\mu_q = 0$ leads to a decrease of the rate [cf. Fig. 8(a)]. However, e.g., for the temperature $T = 0.2$ GeV an increasing μ_q leads to either an increase of the rate (for $\mu_q = 0.2$ GeV) or to the decrease of R (for $\mu_q = 0.3$ GeV). Therefore, the dependence of R on both the medium temperature and quark chemical potential is not trivial. The dependence of the rates on the medium temperature T and quark chemical potential μ_q for a heavy quark with a momentum $p = 5$ GeV is illustrated in Fig. 8(b) in DpQCD. As expected, the rate increases for higher temperatures at $\mu_q = 0$ because the number of plasma particles becomes larger ($\sim T^3$). Therefore, the increase of the interaction rate with temperature keeping μ_q small is seen. For a fixed temperature, the variation

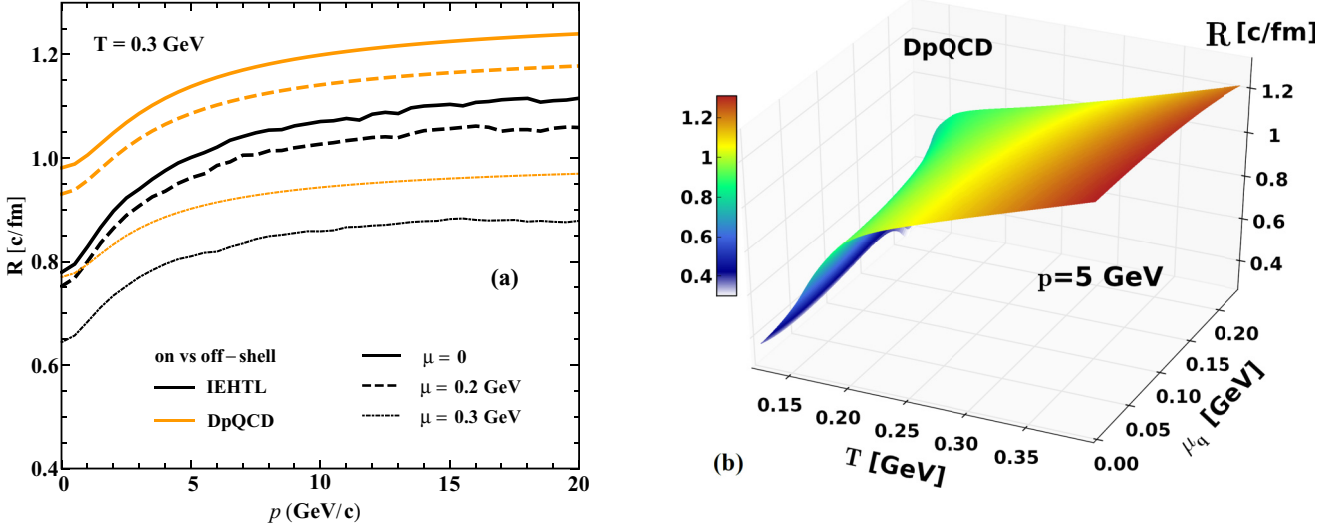


FIG. 8. (Color online) The total elastic interaction rate R of c quarks in the plasma rest frame in the IEHTL and DpQCD models as a function of the heavy quark momentum p for three different values of the quark chemical potential $\mu_q = 0, 0.2, 0.3$ GeV at $T = 0.3$ GeV (a). (b) 3D plot of the total elastic interaction rate R within DpQCD as a function of T and μ_q .

of μ_q leads to different profiles in the rates. A decrease of the total rate for high temperatures when μ_q increases and an opposite trend for small temperatures [$T < T_c(\mu_q = 0)$] is observed. The highest values of the rates are reached for small μ_q and large temperatures T .

Because of the different abundances of particle species in a medium at finite chemical potential, it is interesting to study the variation of the heavy quark interaction rates with the quarks or antiquarks and gluons independently. Figures 9(a)–9(c) illustrate the dependence of the heavy quark collisional rates with quarks, antiquarks, and gluons of a medium at finite temperature T and quark chemical potential μ_q for an intermediate heavy quark momentum ($p = 5$ GeV).

For the case of gluons and antiquarks, the interaction rates are increasing with higher temperature for all μ_q . The charm quark interaction rate with light quarks (R_{uc}) depends on (T, μ_q) in a similar fashion as described in Fig. 8(b) for large μ_q and small temperatures [$T < T_c(\mu_q = 0)$]. Indeed, for larger values of μ_q and small temperatures, R_{uc} is much larger than $R_{\bar{u}c}$ and R_{gc} , so that the total interaction rates are dominated by R_{uc} . On the other hand the R profile is dominated by R_{gc} for small μ_q and large temperatures. This is easy to interpret: At large μ_q the number of light quarks is large compared to the number of antiquarks, i.e., the Fermi-Dirac distribution contributes unequally to R for u and \bar{u} . On the other hand the gluon number decreases with larger μ_q because it is correlated with the subdominant light antiquarks, via the T and μ_q dependencies of the masses.

V. HEAVY QUARK ENERGY LOSS IN A MEDIUM AT FINITE TEMPERATURE T AND CHEMICAL POTENTIAL μ_q

The collisional energy loss dE/dt has been formulated by Bjorken and been explicitly calculated in Ref. [23] for $\mu_q = 0$. We recall here the expression of dE/dt for on- and off-shell

partons. In the framework of the DpQCD model, dE/dt is given in the plasma rest frame by

$$\frac{dE^{\text{on}}}{dt}(p, T, \mu_q) = \frac{M_Q}{4(2\pi)^3} \int_0^\infty \frac{q^4 m_1^{\text{on}}(s)}{s^2 E_q} \times \left[-q f_0(q) + \frac{p}{E} (M_Q + E_q) f_1(q) \right] dq. \quad (5.1)$$

Equation (5.1) is easily extended to the off-shell case with Breit-Wigner spectral functions using (4.4). One finds [23]

$$\frac{dE^{\text{off}}}{dt}(p, T, \mu_q) = \frac{4}{(2\pi)^7} \Pi_{i \in p, q, p', q'} \int m_p m_i dm_i \rho_i^{\text{BW}}(m_i) \int_0^\infty \frac{q^4 m_1^{\text{off}}(s)}{s^2 E_q} \times \left[-q f_0(q) + \frac{p}{E} (M_Q + E_q) f_1(q) \right] dq, \quad (5.2)$$

where $m_1^{\text{on}}(s)$, $m_1^{\text{off}}(s)$, and $f_1(q)$ in (5.1) and (5.2) are given by

$$\begin{aligned} m_1^{\text{on}}(s) &:= \frac{1}{8p_{cm}^4} \int_{-4p_{cm}^2}^0 \frac{1}{8p g_Q} \sum_{i,j} \sum_{k,l} |\mathcal{M}|^2(s, t; i, j | k, l) \\ &\quad \times (-t) dt, \\ m_1^{\text{off}}(s) &:= \frac{1}{4p^i p^f} \int_{t_{\min}}^{t_{\max}} \frac{1}{g_p g_Q} \sum_{i,j} \sum_{k,l} |\mathcal{M}_{2,2}^{\text{off}}(s, t; i, j | k, l)|^2 \\ &\quad \times \left[1 - \frac{t - (M_Q^i)^2 + (M_Q^f)^2 - 2E^i E^f}{2p^i p^f} \right] dt, \\ f_n(q) &= \frac{1}{2} \int d \cos \theta_r f \left(\frac{u^0 E_q - uq \cos \theta_r \mp \mu_q}{T} \right) \cos^n \theta_r. \end{aligned} \quad (5.3)$$

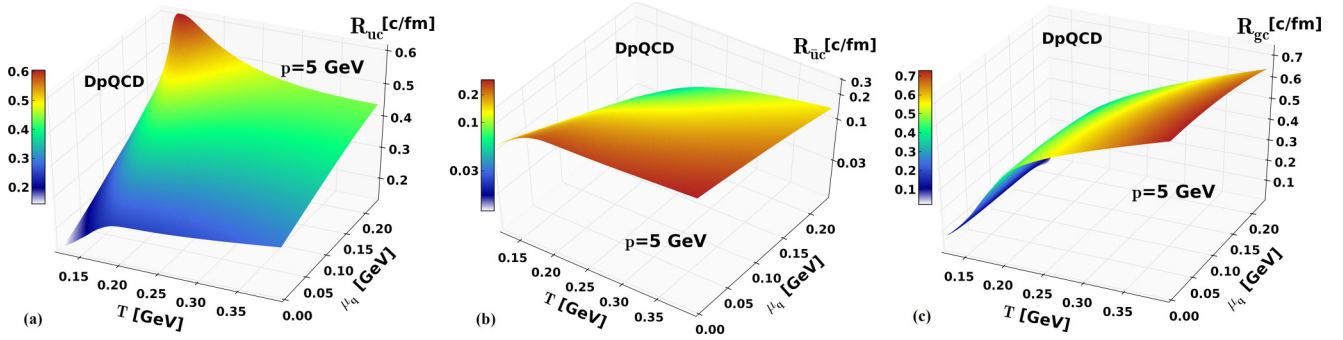


FIG. 9. (Color online) The total elastic interaction rate R of c quarks in the plasma rest frame as a function of the temperature T and quark chemical potential μ_q from the scattering with light quarks (a), light antiquarks (b), and gluons (c). The on-shell heavy quark momentum in all cases is $p = 5$ GeV.

Furthermore, $p^i (M_Q^i)$ is the initial heavy momentum (mass) and $p^f (M_Q^f)$ is the final heavy momentum (mass). The heavy quark energy loss [Eqs. (5.1) and (5.2)] is illustrated in Fig. 10 as a function of the heavy quark momentum for the DpQCD and IEHTL models at $T = 0.2$ GeV for different quark chemical potentials up to $\mu_q = 0.3$ GeV. As for the rates, the off-shell spectral function decreases the energy loss as compared to the on-shell case as described by the DpQCD model. The difference is uniform as a function of the heavy-quark momentum p and the increase of the quark chemical potential. For low heavy-quark momenta and higher medium temperatures, the heavy quark loses less energy by elastic collisions. At low momentum heavy quarks start to gain energy to approach thermal equilibrium and to arrive at the average energy in the heat bath (dE/dx is negative). For a medium at the temperature $T = 0.2$ GeV, the increase

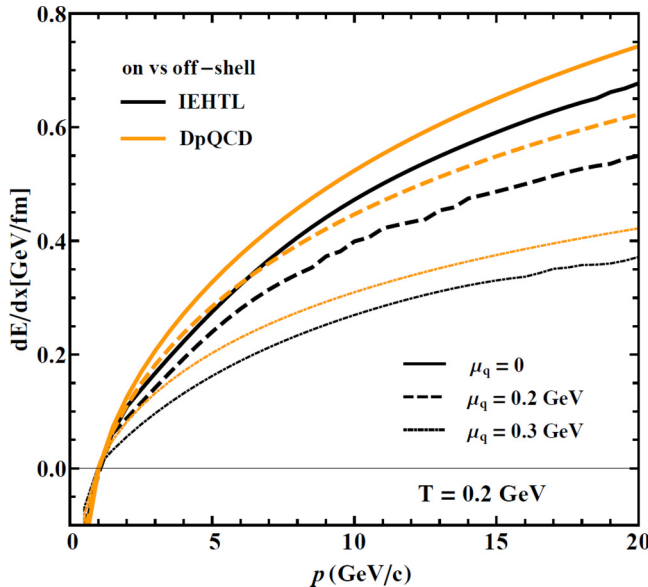


FIG. 10. (Color online) The c -quark energy loss, dE/dx , in the plasma rest frame from the DpQCD and IEHTL models as a function of the heavy quark momentum p at $T = 0.2$ GeV for different values of the quark chemical potential μ_q .

of μ_q leads to a decrease of the heavy quark energy loss. Nevertheless, varying both the medium temperature and μ_q influences the heavy quark energy loss in different ways.

The temperature and quark chemical potential dependencies of the collisional energy loss for low ($p = 1$ GeV/c) and intermediate heavy quark momentum ($p = 5$ GeV/c) is displayed in Figs. 11(a) and 11(b) for the on-shell DpQCD model, respectively. Figures 11(a) and 11(b) show that the energy loss is increasing as a function of p . For intermediate momenta p the conclusions drawn for the rate are valid also for the collisional energy loss; especially Fig. 11(b) shows that with increasing temperature for small values of μ_q —which corresponds to the increase of the parton masses in the DpQCD—the energy loss becomes larger. This is more pronounced for large heavy quark momenta. On the contrary, for $p = 1$ GeV [cf. Fig. 11(a)], where we observe an energy gain (a negative energy loss), the energy gain increases with the distance of the energy of the heavy quark from its equilibrium value. Nevertheless, as expected for a crossover transition (at finite but small values of μ_q) we observe a very smooth dependence of the energy loss on both variables, T and μ_q . The dependencies of dE/dx on T and μ_q are studied in [50] using an extension of finite temperature HTL calculation to include finite μ_q in the distribution functions of the quark/antiquarks. The effect of finite μ_q on dE/dx seen in [50] is much smaller than in our DpQCD and IEHTL models, shown in Fig. 10. We note that the finite μ_q effects in both the parton masses, coupling constant, and distribution function are included in our model, which give to our calculations more inclusive effects than those of [50].

The energy loss of a heavy quark due to its scattering with the QGP partons varies with the abundance of the particle species. Whereas the scattering of heavy quarks on the gluons is slightly μ_q dependent, the scattering on light quarks/antiquarks induces an energy loss which is highly (T , μ_q) dependent. Figures 12(a)–12(c) illustrate this dependence of the heavy quark collisional energy loss with quarks, antiquarks, and gluons of a finite temperature T and quark chemical potential μ_q medium for an intermediate heavy quark momentum ($p = 5$ GeV). As seen for the interaction rate, the profiles observed for the $q(\bar{q})$ - Q collisional energy loss evolve oppositely because of the Fermi-Dirac distribution. As pointed

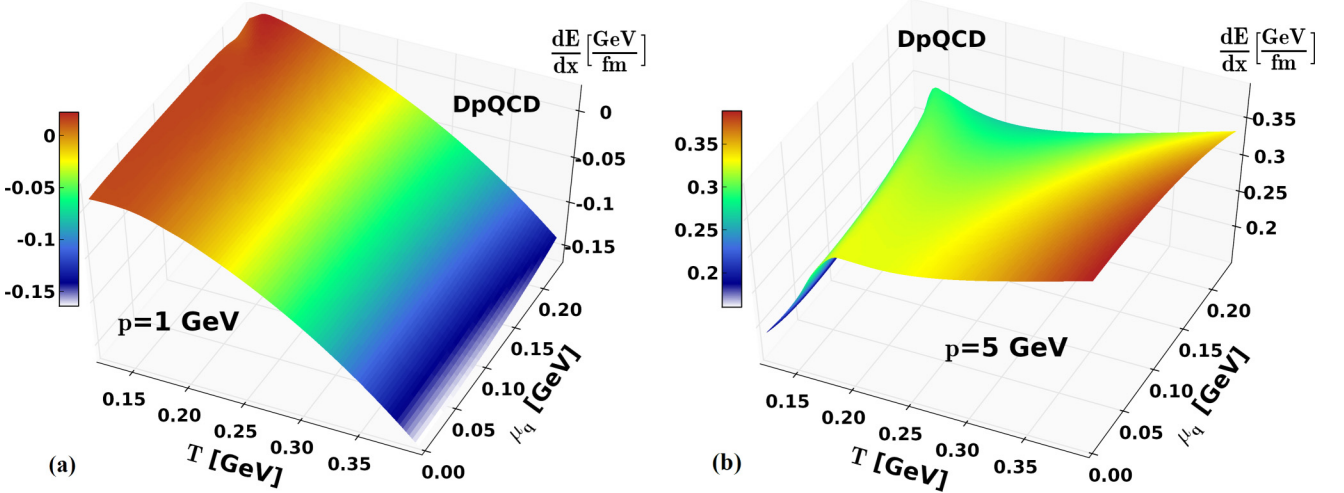


FIG. 11. (Color online) The c -quark energy loss, dE/dx , in the plasma rest frame from the DpQCD approach as a function of the temperature T and quark chemical potential μ_q for the heavy quark momentum $p = 1$ GeV (a) and $p = 5$ GeV (b).

out before, the quark (antiquark) density changes substantially with μ_q .

VI. HEAVY QUARK MOMENTUM LOSS IN A MEDIUM AT FINITE TEMPERATURE AND CHEMICAL POTENTIAL

We continue our study with the momentum loss of heavy quarks in a partonic medium at finite temperature and chemical potential. The drag (A) and diffusion (B) coefficients are evaluated according to [32,58,59] by a Kramers-Moyal power expansion of the collision integral kernel of the Boltzmann equation. Note that the diffusion tensor B admits a transverse-longitudinal decomposition (perpendicular and along the direction of the heavy quark in the fluid rest frame) and contains two independent coefficient B_{\parallel} and B_{\perp} .

A. Longitudinal momentum loss

The drag coefficient A describes the time evolution of the average of the longitudinal component of the momentum transfer $(p - p')^l$ of the heavy quark. For on-shell partons it was defined in the plasma rest frame by Svetitsky [58,59] and

evaluated in [23] by

$$A^{\text{on}}(p, T, \mu_q) = \frac{d\langle p \rangle}{dt} = \frac{M_Q}{4(2\pi)^3} \int_0^\infty \frac{q^4 m_1^{\text{on}}(s)}{s^2 E_q} \times \left[(M_Q + E_q) f_1(q) - \frac{p}{E} q f_0(q) \right] dq. \quad (6.1)$$

Equation (6.1) is easily extended for the off-shell case. One finds [23]

$$A^{\text{off}}(p, T, \mu_q) = \frac{d\langle p \rangle}{dt} = \frac{4}{(2\pi)^7} \Pi_{i \in p, q, p', q'} \times \int m_p m_i dm_i \rho_i^{\text{BW}}(m_i) \int_0^\infty \frac{q^4 m_1^{\text{off}}(s)}{s^2 E_q} \times \left[(M_Q + E_q) f_1(q) - \frac{p}{E} q f_0(q) \right] dq, \quad (6.2)$$

where $m_1^{\text{on}}(s)$, $m_1^{\text{off}}(s)$, and $f_{0,1}(q)$ are given in (5.3).

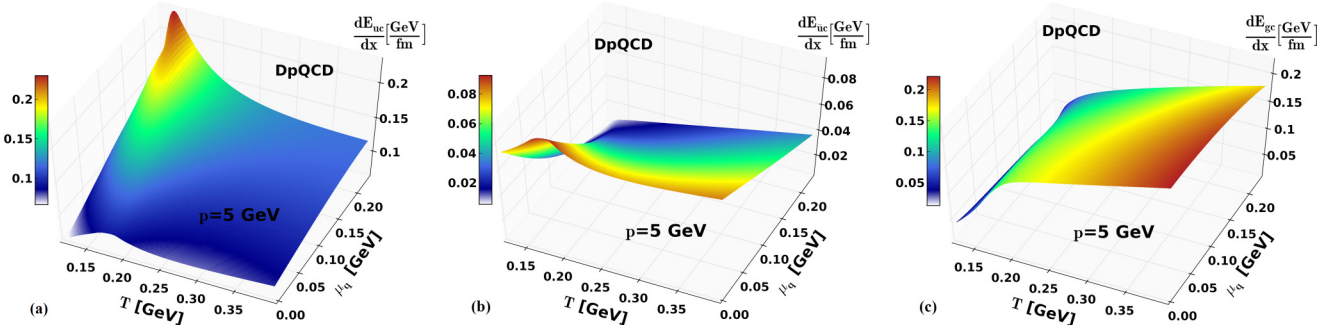


FIG. 12. (Color online) The energy loss dE/dx of c quarks in the plasma rest frame as a function of the temperature T and the quark chemical potential μ_q from the scattering with light quarks (a), light antiquarks (b), and gluons (c). The on-shell heavy quark momentum in this case is $p = 5$ GeV.

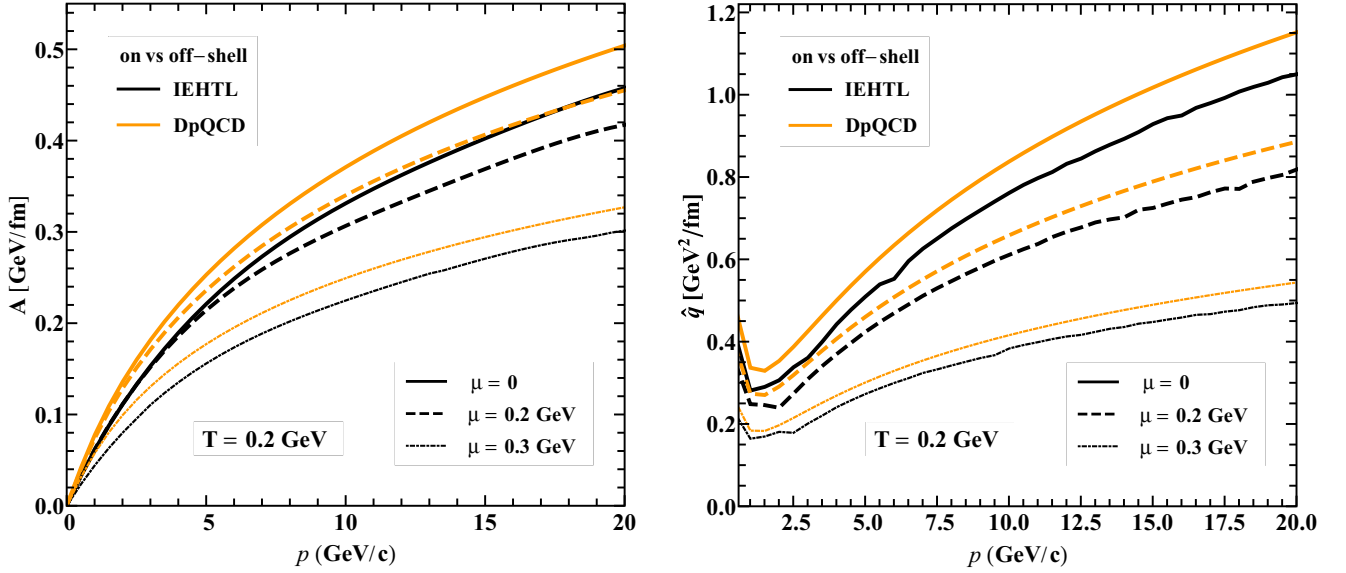


FIG. 13. (Color online) c -quark drag coefficient (6.1) and (6.2) (a), and \hat{q} (6.4) and (6.6) (b) in the plasma rest frame as a function of the heavy quark momentum p for $T = 2$ GeV.

B. Transverse momentum loss

During its propagation through the plasma a heavy quark receives random kicks (momentum transfers) from the constituents of the medium. The average value of the transverse momentum remains zero but the variance $\langle p_{\perp}^2 \rangle$ increases with the number of collisions. The increase of the variance $\langle p_{\perp}^2 \rangle$ per unit length is called the transport coefficient \hat{q} and defined as

$$\hat{q} = \frac{d\langle p_{\perp}^2 \rangle}{dx} = \frac{\langle p_{\perp}^2 \rangle_{\text{single coll}}}{\ell}. \quad (6.3)$$

Using the relation between the transverse second moment B_T and \hat{q} given by $\hat{q} = \frac{4E}{p} B_T$, we can evaluate \hat{q} for massive on-shell partons (as in [23]) by the expression,

$$\begin{aligned} \hat{q}^{\text{on}}(p, T, \mu_q) &= \frac{M_Q^3}{2(2\pi)^3 p} \int_0^{+\infty} \frac{q^5}{s^2 E_q} \left[\frac{m_1^{\text{on}}(s) - m_2^{\text{on}}(s)}{2} \right. \\ &\quad \times (f_0 + f_2) + \left. \frac{(E_q + M_Q)^2}{s} m_2^{\text{on}}(s) (f_0 - f_2) \right] dq, \end{aligned} \quad (6.4)$$

where $m_1^{\text{on}}(s)$ and $f_{0,1,2}(q)$ are given in (5.3) and $m_2^{\text{on}}(s)$ by

$$\begin{aligned} m_2^{\text{on}}(s) &= \int_{-1}^1 d\cos\theta \left(\frac{1 - \cos\theta}{2} \right)^2 \frac{1}{g_g g_Q} \\ &\quad \times \sum_{ij} \sum_{kl} |\mathcal{M}^{\text{on}}|^2(s, t; ij|l, k) \\ &= \frac{1}{32p_{cm}^6} \int_{-4p_{cm}^2}^0 \frac{1}{g_g g_Q} \sum_{ij} \sum_{kl} |\mathcal{M}^{\text{on}}|^2(s, t; ij|l, k) t^2 dt. \end{aligned} \quad (6.5)$$

The off-shell transport coefficient \hat{q}^{off} is deduced by using Breit-Wigner spectral functions for the off-shell partons and extending the on-shell \hat{q}^{on} as

$$\begin{aligned} \hat{q}^{\text{off}}(p, T, \mu_q) &= \frac{1}{2(2\pi)^3} \prod_{i \in p, q, p', q'} \int \frac{m_p^2}{p} m_i dm_i \rho_p^{\text{BW}}(m_i) \\ &\quad \times \int \frac{q^5 m_p}{s^2 E_q} \left[\frac{m_1^{\text{off}}(s) - m_2^{\text{off}}(s)}{2} (f_0 + f_2) \right. \\ &\quad \left. + \frac{(E_q + m_p)^2}{s} m_2^{\text{off}}(s) (f_0 - f_2) \right] dq, \end{aligned} \quad (6.6)$$

with

$$\begin{aligned} m_2^{\text{off}}(s) &= \frac{1}{8p^i p^f} \int_{t_{\min}}^{t_{\max}} \frac{1}{g_g g_Q} \sum_{ij} \sum_{kl} |\mathcal{M}^{\text{off}}|^2(s, t; ij|l, k) \\ &\quad \times \left[1 - \frac{t - (M_Q^i)^2 + (M_Q^f)^2 - 2E^i E^f}{2p^i p^f} \right]^2 dt. \end{aligned} \quad (6.7)$$

C. Numerical results

We discuss now the drag coefficient and the transport coefficient \hat{q} for the models DpQCD and IEHTL from Ref. [39] at finite T and μ_q . In the DpQCD approach, the light and heavy quark and gluon masses are given by the DQPM pole masses. Figure 13(a) shows the drag coefficient (6.1) and (6.2) of heavy quarks as a function of the heavy quark momentum p . The temperature of the heat bath is chosen as $T = 0.2$ GeV. Figure 13(b) illustrates the influence of a finite parton width on the heavy quark transport coefficient \hat{q} , where \hat{q} is displayed for on-shell partons (DpQCD) and off-shell partons (IEHTL) as a function of the heavy quark momentum and for a temperature of $T = 0.2$ GeV and different values of μ_q . For both A and \hat{q} the off-shell parton case is slightly lower by

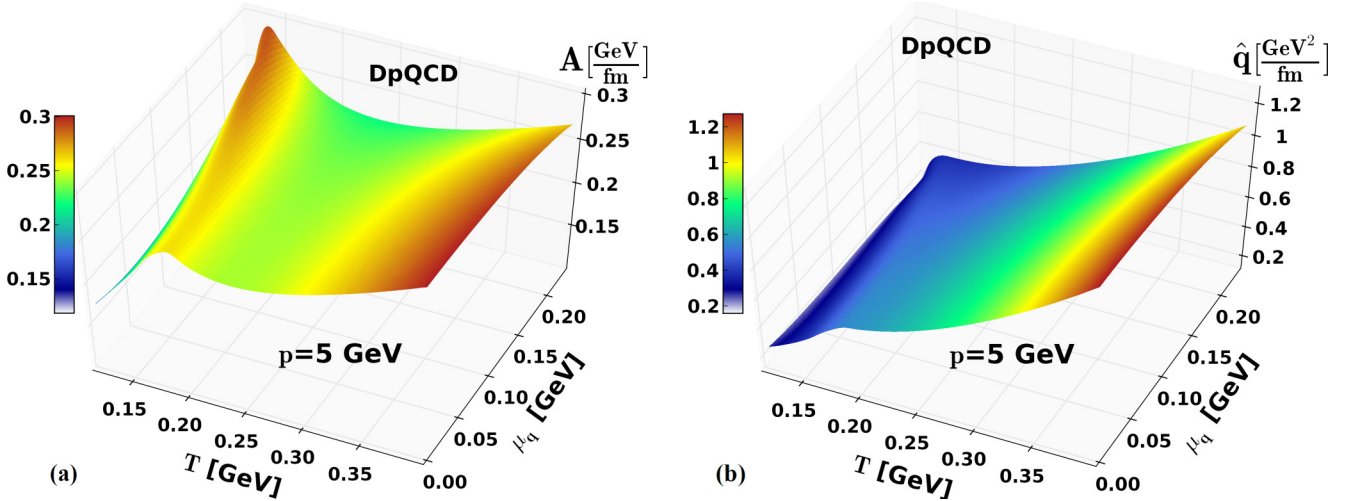


FIG. 14. (Color online) c -quark drag (a) and \hat{q} (b) in the plasma rest frame from the DpQCD approach as a function of the temperature T and quark chemical potential μ_q for the heavy quark momentum $p = 5$ GeV.

about 20% independent of momentum, temperature or quark chemical potential than for the corresponding on-shell case.

The temperature and quark chemical potential dependencies of the drag coefficient and \hat{q} for intermediate heavy quark momentum ($p = 5$ GeV/c) are displayed in Figs. 14(a) and 14(b) for the on-shell DpQCD model, respectively. Figures 14(a) and 14(b) show that both the longitudinal and transverse momentum is increasing for high temperatures and low μ_q . On the contrary, for low temperatures and large μ_q the longitudinal momentum loss is still considerable whereas the transverse momentum transfer is low. We conclude that longitudinal momentum transfers are important not only in a hot medium but also in a dense medium whereas the dense medium leads to less transverse fluctuations in the heavy quark propagation. The relatively large drag at low temperatures in DpQCD/IEHTL is due to the strong increase of the running coupling $\alpha_s(T, \mu_q)$ (infrared enhancement) for temperatures close to $T_c(\mu_q)$.

Regarding the variations in T and μ_q of the longitudinal and transverse momentum losses, one may roughly presage the tendency of the nuclear modification factor R_{AA} and the elliptic flow of charm particles in a hot and dense medium. We expect that the R_{AA} of charmed mesons will still be small in a hot and dense medium as in case of finite temperature and zero chemical potential. On the contrary, the elliptic flow v_2 is expected to be much smaller in a hot and dense medium compared to our knowledge from RHIC and LHC measurements for $\mu_q \approx 0$, because the dense medium damps the transverse momentum fluctuations. Moreover, one could notice that these finite μ_q calculations might have interesting consequences on the c -quark angular correlations at FAIR, which should be more peaked than those seen at RHIC or LHC. However, such predictions have to be confirmed by explicit transport simulations of the finite temperature and chemical potential QGP, because the macroscopic observables (R_{AA} and v_2) depend not only on the microscopic processes and transport coefficients, as studied in this work, but also on the time evolution of the QGP. Such studies will be carried out

in the near future using the Parton-Hardon-String-Dynamics (PHSD) transport approach [40,60] for heavy-ion collisions from $\sqrt{s_{NN}} = 5$ –10 GeV [61].

VII. SUMMARY

We have presented in this work on- and off-shell approaches to describe the microscopic interactions between a heavy quark and the QGP degrees of freedom in a partonic medium at finite temperature T and quark chemical potential μ_q . In our formalism both the perturbative and nonperturbative parts of QCD are involved (DpQCD approach) and an off-shell description of heavy quark interactions in the QGP (IEHTL) at finite T and μ_q . For each of these models, we have calculated the differential cross sections and confronted their implications on the usual mesoscopic observables (energy loss, drag and diffusion coefficients, longitudinal and transverse Q momentum fluctuations, etc.) at finite T and μ_q .

The fundamental parameters describing the heavy quark collisional scattering have been fixed within the DQPM at finite temperature and chemical potential. The formulation of the DQPM at finite μ_q is based on the hypothesis that the phase boundary is close to the line of constant energy density in the (T, μ_q) plane which leads to the approximation (2.5). On the other hand this approximation is in very good agreement with recent IQCD results [53] on the expansion coefficient with respect to μ_q^2 . Accordingly we infer that the equation of state of QCD from $T_c(\mu_q)$ to higher temperatures is roughly under control at least for small/moderate quark chemical potentials.

Our study demonstrates that even if the influence of the finite width of the quasiparticles on heavy quark scattering is small on the off-shell Q scattering cross sections, a noticeable effect is seen in the off-shell transport coefficients (IEHTL model) as compared to the on-shell ones (DpQCD model). This is due to reduced kinematical thresholds in the off-shell cross sections and is independent of the variables (T, μ_q) .

A medium in which the chemical potential is finite leads to a reduction of the qQ and gQ elastic cross section

and consequently to a reduction of heavy quark energy and momentum losses as compared to a zero μ_q medium. Nevertheless, we have concluded that longitudinal momentum transfers are important not only in a hot medium but also in a dense medium whereas the dense medium leads to less transverse fluctuations in the heavy quark propagation. The relative large drag at low temperatures in DpQCD/IEHTL is due to the strong increase of the running coupling $\alpha_s(T, \mu_q)$ (infrared enhancement) for temperatures close to $T_c(\mu_q)$.

We have observed a smooth dependence of the energy loss on both variables T and μ_q at finite but not too large values of μ_q . Such a profile is expected for a crossover transition from the partonic to the hadronic medium. For $\mu_q = 0$ the gluon mass depends on the temperature and therefore the increase of the energy loss is from a change of the coupling. For $\mu_q = 0.2$ GeV, the energy loss is also increasing with temperature but less than for $\mu_q = 0$ because here both the coupling and the effective gluon mass decrease and the increase of the infrared regulator is counterbalanced by the decrease of the coupling. Because the variations of all transport coefficients with T and μ_q are rather smooth (within the present DQPM propagators) the transition from hadronic degrees of freedom to partonic

ones remains a crossover up to $\mu_q = 0.2$ GeV. Present studies within the DQPM indicate a change to a first-order transition only for $\mu_q > 0.3$ GeV but this is still model dependent and not robust.

From the variations of the longitudinal and transverse momentum losses with T and μ_q we expect a large suppression of R_{AA} of charmed mesons in a hot and dense medium, but a much smaller value of the elliptic flow v_2 in a hot and dense medium as compared to our knowledge from RHIC and LHC for finite temperature and approximately zero chemical potential. However, such expectations have to be confirmed by microscopic transport simulations (e.g., within PHSD) for heavy-ion collisions from AGS to SPS energies. This is also the energy regime of the future FAIR and NICA facilities and the BES program at RHIC that all address the properties of QCD at high baryon densities or high μ_q , respectively.

ACKNOWLEDGMENT

H.B. acknowledges financial support from DFG and the “HIC for FAIR” framework of the “LOEWE” program. The computational resources have been provided by the LOEWE-CSC.

-
- [1] F. Weber, *J. Phys. G* **27**, 465 (2001).
 - [2] F. Wilczek, [arXiv:hep-ph/0003183](https://arxiv.org/abs/hep-ph/0003183).
 - [3] P. Braun-Munzinger, *Nucl. Phys. A* **681**, 119 (2001).
 - [4] P. Braun-Munzinger, D. Magestro, K. Redlich, and J. Stachel, *Phys. Lett. B* **518**, 41 (2001).
 - [5] F. Becattini, M. Gazdzicki, A. Keranen, J. Manninen, and R. Stock, *Phys. Rev. C* **69**, 024905 (2004).
 - [6] R. Auerbeck, [arXiv:nucl-ex/9803001](https://arxiv.org/abs/nucl-ex/9803001).
 - [7] J. Cleymans and K. Redlich, *Phys. Rev. Lett.* **81**, 5284 (1998).
 - [8] Z. Fodor and S. Katz, *J. High Energy Phys.* 04 (2004) 050.
 - [9] S. Ejiri, C. R. Allton, S. J. Hands, O. Kaczmarek, F. Karsch *et al.*, *Prog. Theor. Phys. Suppl.* **153**, 118 (2004).
 - [10] I. C. Arsene *et al.*, *Phys. Rev. C* **75**, 034902 (2007).
 - [11] A. Andronic, P. Braun-Munzinger, and J. Stachel, *Phys. Lett. B* **673**, 142 (2009).
 - [12] W. Cassing and E. Bratkovskaya, *Phys. Rept.* **308**, 65 (1999).
 - [13] W. Cassing, E. Bratkovskaya, and A. Sibirtsev, *Nucl. Phys. A* **691**, 753 (2001).
 - [14] A. D. Frawley, T. Ullrich, and R. Vogt, *Phys. Rept.* **462**, 125 (2008).
 - [15] O. Linnyk, E. Bratkovskaya, W. Cassing, and H. Stoecker, *Nucl. Phys. A* **786**, 183 (2007).
 - [16] O. Linnyk, E. Bratkovskaya, and W. Cassing, *Int. J. Mod. Phys. E* **17**, 1367 (2008).
 - [17] T. Matsui and H. Satz, *Phys. Lett. B* **178**, 416 (1986).
 - [18] W. Cassing, E. Bratkovskaya, and S. Juchem, *Nucl. Phys. A* **674**, 249 (2000).
 - [19] A. Andronic, P. Braun-Munzinger, K. Redlich, and J. Stachel, *Phys. Lett. B* **659**, 149 (2008).
 - [20] A. Peshier, *Phys. Rev. D* **70**, 034016 (2004).
 - [21] A. Peshier, *J. Phys. G: Nucl. Part. Phys.* **31**, S371 (2005).
 - [22] W. Cassing, *The European Physical Journal Special Topics* **168**, 3 (2009).
 - [23] H. Berrehrah, P.-B. Gossiaux, J. Aichelin, W. Cassing, and E. Bratkovskaya, *Phys. Rev. C* **90**, 064906 (2014).
 - [24] R. Cutler and D. Sivers, *Phys. Rev. D* **17**, 196 (1978).
 - [25] B. Combridge, *Nucl. Phys. B* **151**, 429 (1979).
 - [26] E. Braaten and M. H. Thoma, *Phys. Rev. D* **44**, R2625 (1991).
 - [27] E. Braaten and M. H. Thoma, *Phys. Rev. D* **44**, 1298 (1991).
 - [28] J. Kapusta, P. Lichard, and D. Seibert, *Phys. Rev. D* **44**, 2774 (1991).
 - [29] A. Peshier, *Phys. Rev. Lett.* **97**, 212301 (2006).
 - [30] A. Peshier, *Nucl. Phys. A* **888**, 7 (2012).
 - [31] S. Peigne and A. Peshier, *Phys. Rev. D* **77**, 114017 (2008).
 - [32] P. B. Gossiaux, V. Guiho, and J. Aichelin, *J. Phys. G* **31**, S1079 (2005).
 - [33] P. B. Gossiaux and J. Aichelin, *Phys. Rev. C* **78**, 014904 (2008).
 - [34] P. Gossiaux and J. Aichelin, *Nucl. Phys. A* **830**, 203c (2009).
 - [35] P. Gossiaux and J. Aichelin, *J. Phys. G* **36**, 064028 (2009).
 - [36] P. B. Gossiaux, R. Bierkandt, and J. Aichelin, *Phys. Rev. C* **79**, 044906 (2009).
 - [37] P. Gossiaux, J. Aichelin, T. Gousset, and V. Guiho, *J. Phys. G* **37**, 094019 (2010).
 - [38] P. Gossiaux, V. Guiho, and J. Aichelin, *J. Phys. G* **32**, S359 (2006).
 - [39] H. Berrehrah, E. Bratkovskaya, W. Cassing, P. Gossiaux, J. Aichelin, and M. Bleicher, *Phys. Rev. C* **89**, 054901 (2014).
 - [40] W. Cassing and E. Bratkovskaya, *Nucl. Phys. A* **831**, 215 (2009).
 - [41] W. Cassing, *Nucl. Phys. A* **791**, 365 (2007).
 - [42] N. Haque, J. O. Andersen, M. G. Mustafa, M. Strickland, and N. Su, *Phys. Rev. D* **89**, 061701 (2014).
 - [43] A. Peshier, B. Kämpfer, O. P. Pavlenko, and G. Soff, *Phys. Rev. D* **54**, 2399 (1996).
 - [44] P. Levai and U. W. Heinz, *Phys. Rev. C* **57**, 1879 (1998).

- [45] A. Peshier, B. Kampfer, and G. Soff, *Phys. Rev. C* **61**, 045203 (2000).
- [46] A. Peshier, B. Kampfer, and G. Soff, *Phys. Rev. D* **66**, 094003 (2002).
- [47] A. Rebhan and P. Romatschke, *Phys. Rev. D* **68**, 025022 (2003).
- [48] E. Braaten and R. D. Pisarski, *Phys. Rev. D* **45**, R1827(R) (1992).
- [49] J. P. Blaizot and E. Iancu, *Nucl. Phys. B* **417**, 608 (1994).
- [50] H. Vija and M. H. Thoma, *Phys. Lett. B* **342**, 212 (1995).
- [51] Z. Fodor, S. Katz, and K. Szabo, *Phys. Lett. B* **568**, 73 (2003).
- [52] R. Marty, E. Bratkovskaya, W. Cassing, J. Aichelin, and H. Berrehrh, *Phys. Rev. C* **88**, 045204 (2013).
- [53] C. Bonati, M. D'Elia, M. Mariti, M. Mesiti, F. Negro, and F. Sanfilippo, *Phys. Rev. D* **90**, 114025 (2014).
- [54] O. Kaczmarek, F. Karsch, F. Zantow, and P. Petreczky, *Phys. Rev. D* **70**, 074505 (2004).
- [55] H. D. Politzer, *Physics Reports* **14**, 129 (1974).
- [56] B. Combridge, J. Kripfganz, and J. Ranft, *Phys. Lett. B* **70**, 234 (1977).
- [57] T. Song, H. Berrehrh, D. Cabrera, J. M. Torres-Rincon, L. Tolos *et al.*, [arXiv:1503.03039](https://arxiv.org/abs/1503.03039).
- [58] B. Svetitsky, *Phys. Rev. D* **37**, 2484 (1988).
- [59] M. G. Mustafa, D. Pal, and D. K. Srivastava, *Phys. Rev. C* **57**, 889 (1998).
- [60] E. Bratkovskaya, W. Cassing, V. Konchakovski, and O. Linnyk, *Nucl. Phys. A* **856**, 162 (2011).
- [61] V. P. Konchakovski, W. Cassing, Y. B. Ivanov, and V. D. Toneev, *Phys. Rev. C* **90**, 014903 (2014).